Coupled-Cluster Studies of Alkylperoxy Radicals: Theory, Properties, and Reactions

by

Andrew Michael Launder

(Under the direction of Henry F. Schaefer III)

Abstract

Air pollution due to emissions from the combustion of fossil fuels is one of the biggest threats to human and environmental health. By interacting with tropospheric particles, complications due to these pollutants may be augmented by chain reactions and dispersive processes. Some of the most important chemical compounds in this regard are peroxy radicals (RO_2), central to both combustion and atmospheric chemistries. Due to the reactive nature of RO_2 and their subsequent reaction products, properties of these species have proven difficult to capture with experiment. High-level *ab initio* methods such as coupled-cluster (CC) theory have thus emerged as a complementary tool to experimental work on RO_2. Herein, we report CC studies on the reactions and properties of RO_2. First, we report work on the reactants, products, intermediates, and transition states of CH_3O_2 + NO, providing highly reliable predictions of the reaction mechanism. Then we investigate the $\tilde{X}$ and $\tilde{A}$ states of the conformers of $C_2H_5O_2$, reporting properties of spectroscopic relevance (such as transition origins and fundamental vibrational frequencies).

Index words: Combustion, tropospheric chemistry, alkylperoxy radicals, radical-radical reactions, electronic structure theory, coupled-cluster theory, focal point approach, excited electronic states

Coupled-Cluster Studies of Alkylperoxy Radicals: Theory, Properties, and Reactions

by

Andrew Michael Launder

B.S., George Fox University, 2013

A Dissertation Submitted to the Graduate Faculty
of The University of Georgia in Partial Fulfillment
of the
Requirements for the Degree

Doctor of Philosophy

Athens, Georgia

2017

Coupled-Cluster Studies of Alkylperoxy Radicals: Theory, Properties, and Reactions

by

Andrew Michael Launder

Approved:

Major Professors: Henry F. Schaefer III

Committee: Gary E. Douberly
Geoffrey D. Smith

Electronic Version Approved:

Dr. Suzanne Barbour
Dean of the Graduate School
The University of Georgia
May 2017

Acknowledgments

" '[Y]ou've got to swim whether you're thrown into a swimming bath or into the middle of the sea.' " – Plato, *The Republic*[1]

An enduring optimism helped to keep me afloat over the course of my scientific career, an idealism that would not have been possible without the aid of the many teachers, friends, and family members who encouraged and assisted me throughout my education. I am not self-sufficient, and have yielded myself, bit by bit, to the knowledge, love, and support of others.

In the course of my secondary education, several of my teachers were instrumental in developing my love of learning. The three that stand out in my memory above others are Drea Ferguson, Doug Geygan, and Pam Mears, though every one of my instructors has shaped my current worldview in a constructive manner. My science and mathematics teachers also deserve special recognition for their encouragement to pursue my strengths. Thank you all for everything that you have done for me and for putting up with my antics.

George Fox University provided me with exceptional preparation for my graduate studies and scientific career. I credit Robin Baker and the many employees and academics at GFU for this, and I am compelled to name every one of my chemistry instructors: Profs. Davida Brown, Paul Chamberlain, Carlisle Chambers, Michael Everest, and Jeff Vargason; as well as Profs. Bob Hamilton and Jim Smart. I feel that the magnitude of their impact speaks to

the strength of the STEM departments at GFU, and I am thankful to their continued and lasting support.

The employees, professors, and graduate students in the University of Georgia's Department of Chemistry and CCQC provided a simultaneously relaxed and rigorous atmosphere in which to research. Discussions with those affiliated with other universities has made clear to me that this balance is very difficult to strike, and I feel blessed to have profited intellectually from this learning environment. The friendships that I have developed here, particularly those with Megha Anand, Andreas Copan, Vickie Lim, Bryan Soto, Jonathon Vandezande, and the Zimmerman family, are invaluable to me, and I attribute many of my successes to them. I also wish to thank my teachers of physical chemistry, particularly Drs. Jay Agarwal, Alex Sokolov, and Justin "Jet" Turney; and Profs. Wesley Allen, Gary Douberly, Paul Schleyer, and Geoffrey Smith. Most of all, I acknowledge my research advisor, Prof. Henry Schaefer. My graduate education would have been incomplete without his kind and energetic personality, his willingness to provide assistance and support, and his exceptional knowledge of chemistry. I am thankful that he accepted me into his group and I am forever indebted to his influence.

Outside of my education, I am eternally grateful for my family, who have provided me with everything I could ask for over the course of my life. I thank my grandparents and extended family for being steadfast and aspirational presences from birth. I thank my brother Robby and his wife Irene for being such good-humored and caring individuals. I thank my parents, Mike and Lori, for filling their house with books, for being the best teachers of all, for supporting and looking after me, and for their incredible love.

One person above all others deserves my love and gratitude. I will never take for granted my good fortune in meeting my wonderful wife, Maria. She was who I came home to every night (or morning, as the case often was). She left her family and friends 2600 miles away to be with me and support me through my biggest and most mentally taxing accomplishment.

She is hilarious, fierce, kind, caring, loyal, selfless, and continually exceeds every one of my wildest expectations for a life partner. I love you forever, Maria, and I look forward to our future together.

Finally, and most importantly, I thank the Lord. I am eternally led to improve myself in His esteem.

Preface

Chemists rationalize the importance of their work by referring to their discipline as the "central science."* The centrality to which they refer is the relative position of chemistry in a schematic representation of the subfields of science. On one side of the fence grows the tree of life sciences, the branches of which ultimately return to biology. On the other is the study of the nature and laws of the inanimate world: physics, the roots of which are the mathematics that underpin the vernacular by which physicists describe their observations. Chemistry, the study of the composition and properties of atoms and molecules, is considered uniquely situated to smoothly interface to both physics and biology, serving as the connecting bridge.

This sort of *linear* thinking breaks down upon closer inspection: the vast and nuanced knowledge base of science may not be reduced to such a simplistic structure. The often collaborative nature of modern research and consequent proliferation of bi- and tridisciplinary subfields (e.g., biophysics, physical biochemistry, etc.) bespeak a complex *web* by which science may be more accurately characterized. Those who specialize in chemistry are no longer free to shut themselves off to other nodes of the scientific web; by necessity, they develop some degree of interdisciplinary character. This not only facilitates and strengthens preexisting connections, but forges new ones.

Computational chemistry has consequently emerged as a field intrinsically linked to multiple disciplines of science. Computational chemists are well acquainted with not only chem-

*One popularizer of this moniker is the widely-used introductory textbook of Brown et al., *Chemistry: The Central Science*, now in its 14th edition.[2]

istry, but with physics, mathematics, and computer science (as specific research requires, they may also be familiarized with others, such as biology, earth science, or astronomy). The term *molecular science*[†] provides a succinct description of this specialized network of overlaps, of which computational chemistry is a key component. Molecular science encompasses the diverse approaches to studying the atoms and bonds that constitute molecules, and it provides the philosophical scaffolding by which many scientists, especially computational chemists, should seek to structure their research.

This monograph is thus best regarded as an investigation of the molecular science of peroxy radicals: the characterization of their properties and reactions via electronic structure theory, as interfaced with thermodynamics, spectroscopy, and atmospheric and combustion chemistries.

[†]The books in the Cambridge Molecular Science series include an excellent series preface which prescribes the use of this term (see, for example, Ref. 3).

Table of Contents

Chapter 1

Introduction and Literature Review

The interplay of combustion emissions with tropospheric compounds originating from biogenic or other anthropogenic sources presents scientific challenges of paramount importance. The continued reliance on fossil fuels (which still account for $> 80\%$ of the world's primary energy demand)[4] ensures that problems stemming from combustion byproducts will continue to plague human health – both directly, via respiratory ailments, and indirectly, via ecological consequences (such as reduction in crop yields).[5,6] In 2012 alone, 6.5 million deaths were attributed to the joint effects of indoor and outdoor air pollution.[7] Air pollutants, as well as interacting species which serve to augment or distribute these pollutants via intricate reaction systems, are of vital interest in this regard.

Peroxy radicals (RO_2; where R is either an H atom or an organic radical) are among the most important chemical compounds observed in these contexts – "hub" molecules that play an integral role in both combustion and tropospheric chemistries. In internal combustion engines, RO_2 species largely originate from autoxidation, the spontaneous, often low-temperature (500 – 1000 K) oxidation of organic material in the presence of O_2.[8,9] Autoxidation has proven an industrial frustration, the cause of not only the pre-ignition and subsequent knocking phenomena in engine cylinders, but also due to deterioration of petrochemical-based products.[10] Indeed, due to dependencies on fuel composition and en-

gine design, autoxidation processes fundamentally limit the efficiency at which a given engine may operate.[11] The desire to improve upon this efficiency merits a deeper understanding of these chemical causes and effects behind current engine limitations.

The initiating step to autoxidation is the abstraction of an H atom from a (sometimes substituted) closed-shell hydrocarbon, resulting in an organic radical. The abstracting agent is typically a hydroxyl radical, OH (which produces H_2O), or O_2 (which produces HO_2, the simplest RO_2 compound).[12] A chain-propagating step follows the initiation reaction, in which the resultant radical reacts with O_2 to form a RO_2 radical.[8,10]

$$R + O_2 \leftrightharpoons RO_2 \qquad \textbf{1.1}$$

Combustion systems are dominated by RO_2 chemistry in the low-temperature regime, largely because of the equilibrium of reaction **1.1**, which favors the product at temperatures below $\sim$ 750 K (depending on R group – this threshold trends lower for RO_2 species with weak R–O bonds).[13] Because of their ubiquitous presence in low-temperature combustion, RO_2 radicals are intimate players in autoxidation processes, where they function as both facilitators (by participating in chain-propagating steps) and inhibitors (by reacting with subsequent byproducts in chain-terminating steps).[8] In one key process, RO_2 radicals undergo intramolecular H atom abstraction, isomerizing to a QOOH radical.[9]

$$RO_2 \leftrightharpoons QOOH \qquad \textbf{1.2}$$

QOOH species permit further chain-propagating steps, which may ultimately result in chain-branching increases in reactive radical initiators.[9]

In juxtaposition to this chemistry are chain-terminating reactions – O_2 may instead abstract a second H atom from R, resulting in HO_2 and a conjugate alkene.[9] It is worth noting here that the smallest RO_2 compounds, HO_2 and CH_3O_2, are relatively inert in

low-temperature combustion, and are thus considered open-shell chain terminators.[14] Their size precludes chain propagation via reaction **1.2**, and the equilibrium of their initiation reaction (i.e., reaction **1.1**) favors the RO_2 product at higher temperatures than most other radicals.* Thus the most interesting chemistry involving these two RO_2 species occurs upon their emission into the troposphere, where they may interact with particles not abundant in low-temperature combustion environments.

Autoxidation in the troposphere is initiated primarily by OH radicals.[6,13,15–17] Due to high concentrations of O_2, products of this initiation step often undergo reaction **1.1** to produce RO_2. Upon further reaction, RO_2 may regenerate OH, which may then serve as an initiator to additional RO_2 production.[13] In the range of temperatures observed in the troposphere, RO_2 largely participates in reactions with other radicals. In clean (unpolluted) air, these include other RO_2 species (which usually results in chain termination via the production of long-lived, closed-shell sinks)[16–19] or, in maritime environments, halogen monoxides.[17,18] In urban (polluted) contexts, however, RO_2 typically reacts with open-shell nitrogen oxides: NO, NO_2, or NO_3.[13]

NO and NO_2 are collectively referred to as NO_x, distinguished by their impact on daytime tropospheric chemistry. NO_x species are primary constituents of photochemical smog, and are the only known natural means of producing tropospheric ozone (O_3).[15,16,20]

$$NO_2 \xrightarrow{h\nu} NO + O(^3P) \qquad \textbf{1.3}$$

$$O(^3P) + O_2 + M \longrightarrow O_3 + M^* \qquad \textbf{1.4}$$

$$NO + O_3 \longrightarrow NO_2 + O_2 \qquad \textbf{1.5}$$

Perturbations of this photostationary state have a profound impact on ambient concentrations of O_3, which is considered an air pollutant in the troposphere.[6,15,16,20] Cou-

*Walker and Morley[14] give "ceiling temperatures" (i.e., the temperature at which $[R] = [RO_2]$ in 0.1 atm O_2) of 1920 and 930 K for R = H and CH_3, respectively.

pled with its well-known role in stratospheric protection from harmful UV radiation,[21–23] O_3 has been characterized as "both the most important and the most paradoxical trace gas in the atmosphere."[24] Via a photocatalyzed two-step process, O_3 is also a principal source of OH initiators in the troposphere and therefore indirectly drives autoxidation processes.[6,15,16,20,21,23,25] These considerations motivate research into the mechanisms and properties of reactions involving photochemical smog species. Reactions with NO_3, on the other hand, are largely relegated to the night (when NO_3 is regenerated via the slower oxidation of NO_2 by O_3).[6,15–17,20,23,26] In the daytime, NO_3 is rapidly photolyzed to produce NO and NO_2,[6,15,16,20,23,26] which further feed reactions **1.3** – **1.5**.

Since tropospheric autoxidation typically requires radicals produced by an initiating photochemical reaction, RO_2 production peaks diurnally and is therefore most relevant to daytime chemistry. Via its reactions with NO_x, RO_2 upsets the photochemical balance of reactions **1.3** – **1.5** and is thus intimately tied to tropospheric $[O_3]$.[13,16–18,21,23,25] Because of this, RO_2 + NO_x has been frequently cited as a key reaction class requiring further research and analysis.[13,19,23] However, complex multichannel schemes and the rapid rates of many of the resultant reactions complicate matters.[13,16,18,27] Because of these experimental challenges, much of this chemistry may be more easily captured with theory.

High-level *ab initio* computational methodologies are particularly well-suited to this task. In particular, coupled-cluster theory with single, double, and perturbative triple excitations [CCSD(T)] has been shown to capture much of the dynamic electron correlation that zeroth-order Hartree-Fock approximations are unable to describe for single-reference problems (higher excitations in CC theory are even able to systematically recover multireference character). Pairing CCSD(T) with large atomic orbital basis sets often provides such a good balance of accuracy and computational effort that this level of theory has been referred to as the "gold standard" of electronic structure theory. However, the many reactions occurring on various timescales that arise from the interactions of often multiple isomers of myriad

chemical species of widely varying size provide such a complex and vast web of interactions that kinetic modeling routines are frequently employed to describe climate[19] and combustion[12,14,28–30] processes approaching macroscopic scale. Yet to provide even qualitative accuracy, these modeling algorithms are implicitly dependent on *ab initio* methods to predict accurate molecular properties, which may then be used to derive reaction mechanisms, thermochemical parameters, rate constants, and branching ratios. Electronic structure and kinetic modeling computations thus provide experimentalists with predictive or corroborative data that makes theory an indispensible tool in modern research.

Herein, we provide a representative selection of RO_2 properties and reactions as predicted by CC theory. In Chapter 2, we explore the CH_3O_2 + NO system, a prototypical RO_2 + NO_x reaction. We use CC theory incorporated into the composite focal point approach (FPA) scheme to provide highly reliable reactant, product, intermediate, and transition state enthalpies at 0 K. This allows us to address and refine one of the key areas in which computations can assist atmospheric chemistry: the determination of accurate radical-radical reaction mechanisms.

Our work on $C_2H_5O_2$ (Chapter 3) holds relevance to both combustion and atmospheric chemistries, but especially to spectroscopy. We demonstrate the power of CC theory to reliably capture not only ground state properties of RO_2, but also ones arising from chemical species in excited electronic states. We once again use CC theory to provide sets of extrapolatable energies for FPA predictions of enthalpies 0 K, which are then used to determine $\tilde{A} \leftarrow \tilde{X}$ transition origins. We further report fundamental transitions predicted via second-order vibrational perturbation theory. The principal objective of this monograph is thus to substantiate the suitability and versatility of CC theory in elucidating RO_2 chemistry.

Chapter 2

Exploring Mechanisms of a Tropospheric Archetype: $CH_3O_2 + NO$*

*A. M. Launder, J. Agarwal, and H. F. Schaefer *J. Chem. Phys.*, **2015**, 143, 234302. Reprinted here with permission of the American Institute of Physics.

2.1 Abstract

Methylperoxy radical (CH_3O_2) and nitric oxide (NO) contribute to the propagation of photochemical smog in the troposphere via the production of methoxy radical (CH_3O) and nitrogen dioxide (NO_2). This reaction system also furnishes trace quantities of methyl nitrate (CH_3ONO_2), a sink for reactive NO_x species. Here, the CH_3O_2 + NO reaction is examined with highly reliable coupled-cluster methods. Specifically, equilibrium geometries for the reactants, products, intermediates, and transition states of the ground-state potential energy surface are characterized. Relative reaction enthalpies at 0 K (ΔH_{0K}) are reported; these values are comprised of electronic energies extrapolated to the complete basis set limit of CCSDT(Q) and zero-point vibrational energies computed at CCSD(T)/cc-pVTZ. A two-part mechanism involving CH_3O and NO_2 production followed by radical recombination to CH_3ONO_2 is determined to be the primary channel for formation of CH_3ONO_2 under tropospheric conditions. Constrained optimizations of the reaction paths at CCSD(T)/cc-pVTZ suggest that the homolytic bond dissociations involved in this reaction path are barrierless.

2.2 Introduction

In the troposphere, ephemeral organic radicals are involved in the formation of O_3, NO, and NO_2, principal components of photochemical smog. A key subset of this chemistry involves peroxy radicals (RO_2), which are capable of oxidizing NO_x to generate O_3 via[13,18,20,21]

$$RO_2 + NO \longrightarrow RO + NO_2 \qquad \textbf{2.1}$$

$$NO_2 \xrightarrow{h\nu} NO + O(^3P) \qquad \textbf{2.2}$$

$$O(^3P) + O_2 + M \longrightarrow O_3 + M^* \qquad \textbf{2.3}$$

(cf. reactions **1.3** – **1.5**). This sequence of reactions propagates smog formation by adding O_3 to the lower atmosphere, where it negatively affects human health and contributes to tree and crop damage.[6,16] Indeed, virtually all O_3 produced in the troposphere is due to the photolysis of NO_2,[15] which bolsters the importance of a quantitative understanding of reactions **2.1** – **2.3**.

In reaction **2.1**, RO_2 can yield NO_2 through interaction with NO. This process directly influences ambient concentrations of O_3 via reactions **2.2** and **2.3**. NO_2 also originates from the alkoxy (RO) products of **2.1**, because RO yields HO_2 from rapid reaction with molecular oxygen, leading to additional NO_2 formation via HO_2 + NO (reaction **2.1**, R = H).[13,18,23,31] Moreover, RO compounds can form thermally stable adducts with NO_2 (i.e., $RONO_2$), leading to the distribution of O_3 to unpolluted areas via the photolysis of $RONO_2$ into RO + NO_2.[13,21]

Much of the research in understanding peroxy radical chemistry is obfuscated by the fleeting nature of these compounds, causing disagreements and large uncertainties in the underlying reaction mechanisms and kinetic rates. To fully assess the complex chemical and physical interactions in the atmosphere, global chemical transport models require accurate data for tropospheric reactions.[19] The ability of computational quantum chemistry to provide the desired level of accuracy for transient species makes it an excellent complementary approach to experimental work. Herein, we have investigated the CH_3O_2 + NO system (Fig. 2.1), a model reaction within the RO_2 + NO reaction class, and a system that has been identified[19,23,32] as requiring reliable theoretical analysis.

The CH_3O_2 + NO system has been previously examined with both theory[33–45] and experiment.[46–69] Prior work suggests two principal reaction pathways, both of which share a short-lived, vibrationally-excited methyl peroxynitrite intermediate, $[CH_3OONO]^*$ (reaction **a**, see Fig. 2.1). This intermediate complex has not been isolated, but Ravishankara and coworkers[57] note that it explains the small negative temperature dependence observed in the

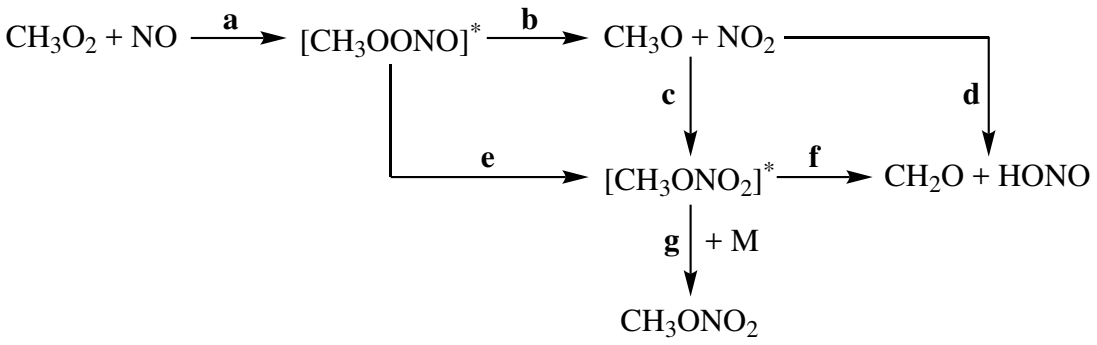

Figure 2.1: Reaction channels in the CH_3O_2 + NO reaction system.

rate expression. In 2003, Lohr, Barker, and Shroll[35] provided the first theoretical account of CH_3OONO using density functional theory (DFT). They found two distinct conformers of this intermediate: *cis*-perp CH_3OONO and *trans*-perp CH_3OONO, where *cis* and *trans* describe the OONO dihedral angle and perp defines the orientation of the OONO moiety with respect to the CH_3 group (i.e., the OONO "plane" is approximately *perp*endicular to the OCH planes).

Following process **a** (Fig. 2.1), $[CH_3OONO]^*$ may either dissociate into CH_3O + NO_2 (reaction **b**) or isomerize to methyl nitrate, $[CH_3ONO_2]^*$ (reaction **e**). Much research has focused on the $k_\mathbf{e}/k_\mathbf{b}$ branching ratio; the current consensus is that the reaction proceeds principally through product channel **b**. That is, the $[CH_3OONO]^*$ complex will either immediately decompose back to the reactants or, upon distribution of excess vibrational energy, cleave the OO bond and form CH_3O and NO_2. Indeed, some studies[38,42,47] have implied a virtually nonexistent probability of reaction **e** for R = CH_3. Note that the $k_\mathbf{e}/k_\mathbf{b}$ ratio is known to increase with the size of R, and channel **e** becomes nonnegligible for R groups containing at least two carbon atoms.[13,23,70–72]

Using infrared spectroscopy and gas chromatography, Pate, Finlayson, and Pitts (1974)[47]

dismissed channel **e** for R = CH_3. They concluded that CH_3O and NO_2 were the only observed products (channel **b**) and that CH_3ONO_2 forms solely via channel **c**. Further work[61–63,65,67–69] confirmed the predominance of channel **b**, but did not exclude the possibility of a small branching ratio with respect to channel **e**. Utilizing observed kinetic data from several RO_2 + NO reactions (R = C_nH_{2n+2}, n = 3 – 8), Carter and Atkinson (1989)[73] developed an expression for determining branching ratios in RO_2 + NO systems. Using recommended values[72] for coefficients in this expression at 300 K and 760 Torr, the branching ratio for R = CH_3 ($k_\mathbf{e}/k_\mathbf{b}$) is 0.37%. Most recently, Butkovskaya, Kukui, and Le Bras (2012)[69] reported a ratio of 1.0 ± 0.7% over the range of temperatures and pressures expected in the troposphere. In fact, it has been suggested that reaction **e** need only occur 0.05% of the time to significantly contribute to global steady-state concentrations of CH_3ONO_2.[74] Additional tropospheric CH_3ONO_2 arises from emissions in the manufacture of explosives[75] and from biogenic marine sources.[76]

Theoretical research has also explored the possibility of reaction **e**. DFT computations with the B3LYP functional and 6-311++G** basis set predict a large activation barrier for the isomerization of *cis*-perp CH_3OONO to CH_3ONO_2 (33 kcal mol^{-1}).[35] However, more recent theoretical work[38,42] suggests that isomerization occurs exclusively by dissociation of *cis*-perp CH_3OONO to the radical products of **b**, followed by barrierless recombination to CH_3ONO_2 (i.e., reaction **c**). In a 2004 study, Zhao, Houk, and Olson[38] reasoned that this is due to the lower barrier for conformational isomerization of *trans*-perp CH_3OONO relative to nitrate isomerization (10 kcal mol^{-1} and 33 kcal mol^{-1}, respectively, using the composite CBS-QB3 methodology). Using the composite G3 methodology, Lesar and coworkers (2006)[41] computed a barrier of less than half of the value reported by Zhao and coworkers (15 kcal mol^{-1} for *trans*-perp $CH_3OONO \rightarrow CH_3ONO_2$). They argue that this would indeed be competitive with their computed barrier for conformational isomerization (11 kcal mol^{-1} for *trans*-perp $CH_3OONO \rightarrow$ *cis*-perp CH_3OONO).

In 2008, Arenas and coworkers[42] constructed potential energy surfaces (PESs) with complete active space second-order perturbation theory (CASPT2), concluding that single-determinant DFT characterizations are insufficient to describe the CH_3O_2 + NO reaction system. They suggested that, due to the warping of the ground-state PES by conical intersections in the vicinity of the CH_3OONO and CH_3ONO_2 dissociation and isomerization reaction paths, certain transition states found by previous studies are purely artifactual. The presence of these conical intersections may be traced to the electronic structure of the ONO moiety. Citing work on the model isomerization of *trans*-FONO $\rightarrow$ FNO_2,[77] Zhao and coworkers[38] noted that the ONO fragment of dissociating CH_3OONO has an electronic and geometric structure akin to the $\tilde{A}\ ^2B_2$ excited state of NO_2. They proposed that the dissociation of *cis*-perp CH_3OONO to the radical products occurs concurrent with the relaxation of the $^2B_2$-like ONO group to the $^2A_1$ ground state of NO_2. This avoided crossing suggests significant multireference character and serves to further lower the energetic barrier to dissociation, allowing the radical products to form.

The secondary reaction channels of CH_3O + NO_2 have also been addressed extensively by experimental studies,[49,78–92] and some uncertainty surrounds the mechanism of formaldehyde (CH_2O) and nitrous acid (HONO) formation. Two possibilities exist: i) direct abstraction (channel **d**); or ii) recombination of CH_3O + NO_2 via reaction **c**, followed by dissociation of $[CH_3ONO_2]^*$ (channel **f**). However, a transition state for direct abstraction has thus far eluded theoretical characterization.[92] Lohr and coworkers[35] reported B3LYP/6-311++G** barriers for the dissociation reactions of CH_3ONO_2 and *cis*-perp CH_3OONO to CH_2O and HONO, predicting them to be too large to significantly contribute to the presence of these two species in the troposphere (38.9 kcal mol^{-1} and 39.1 kcal mol^{-1}, respectively). This conclusion has been supported by further theoretical work.[40,41]

Many of the theoretical studies performed to date on this system have been limited to modest levels. Here we report high-level computations on the CH_3O_2 + NO reaction system.

Relative energies were obtained by focal-point extrapolation to the complete basis set (CBS) limit up to coupled-cluster theory with single, double, triple, and perturbative quadruple excitations [CCSDT(Q)]. From these predictions we determine that the two-part mechanism involving reaction **b** followed by reaction **c** is the primary channel of CH_3ONO_2 formation. By sampling the CCSD(T)/cc-pVTZ reaction paths via constrained geometry optimizations, it is also found that homolytic bond dissociations in the CH_3O_2 + NO reaction system are barrierless.

2.3 Theoretical methods

Optimized geometries for the stationary points were obtained using coupled-cluster theory with single, double, and perturbative triple excitations [CCSD(T)].[93–98] All atoms were described with the correlation-consistent valence triple-ζ (cc-pVTZ) basis sets developed by Dunning.[99] Consistent with the design of these basis sets, a frozen core (FC) approximation was applied: the 1s-like electrons on the C, N, and O atoms were excluded from post-Hartree-Fock computations. Harmonic vibrational frequencies were obtained at the same level of theory as the geometry optimizations. For closed-shell species, a restricted Hartree-Fock (RHF) reference was employed, while an unrestricted formalism (UHF) was used for open-shell species. The quality of the UHF reference was assessed by determining the deviation of $\langle \hat{S}^2 \rangle$ from the physically correct value of 0.75 for doublets. The largest deviation encountered was less than 0.03, indicating a relatively small error due to spin contamination. Optimized structures were verified as local minima or transition states by vibrational analyses; intrinsic reaction coordinate (IRC) computations were performed at the MP2/cc-pVTZ level of theory to ensure that transition state structures connected to the expected minima.

The relative electronic energies (ΔE_e) for all species, with respect to the reactants (CH_3O_2 + NO), were determined using the focal point approach (FPA).[100–103] Up to the CCSD(T) level of theory, absolute electronic energies were systematically extrapolated to the CBS

limit by means of a three-parameter exponential function[104] and a two-parameter power function[105] for the Hartree-Fock and correlation energies, respectively. Additive corrections were included for higher excitations in CC theory [up to CCSDT(Q)].[106–108]

Several corrections were appended to the extrapolated electronic energies to ensure reliable predictions. Corrections to account for the FC approximation (Δ_{core}) were computed as

$$\Delta_{\text{core}} = E(\text{AE-CCSD(T)/cc-pCVTZ}) - E(\text{FC-CCSD(T)/cc-pCVTZ}) \tag{2.4}$$

where AE stands for "all-electron" (all electrons are considered in post-Hartree-Fock computations). The cc-pCVTZ basis is an analog to the cc-pVTZ basis described above, but contains additional basis functions to describe core correlation.[109] Diagonal Born-Oppenheimer corrections (Δ_{DBOC}) were computed at the HF/cc-pVTZ level of theory to account for the clamped nuclei approximation.[110,111] Corrections for scalar relativistic effects (Δ_{rel}) were computed at the AE-CCSD(T)/cc-pCVTZ level of theory and included mass-velocity and Darwin one- and two-electron terms.[112–114] Finally, reaction enthalpies at 0 K ($\Delta H_{0\text{K}}$) were determined by appending the difference in zero-point vibrational energies (Δ_{ZPVE}) obtained from harmonic frequency computations.

The zero-point vibrational energies of open-shell systems were computed with a restricted open-shell (ROHF) reference. This choice is a result of the anomalously large values obtained with a UHF reference for the asymmetric stretch, ω_3, of NO_2 and for ω_e of NO (all other results obtained with a UHF reference agreed to within 3 cm^{-1} of the values obtained with a ROHF reference). These spurious results are due to orbital instability envelopes, which are known to present issues for NO_2[115,116] and NO.[117] Near singularities in the orbital rotation Hessian of the UHF reference determinant manifest themselves as "instability volcanoes" in CC theory.[118] Comparative data for NO_2 and NO is displayed in Table 2.4 in Sect. 2.8.

Throughout, the $\mathcal{T}_1$ diagnostic was employed as a metric to gauge multireference character:[119,120]

$$\mathcal{T}_1 = \sqrt{\frac{|\mathbf{t}_{1\alpha}|^2 + |\mathbf{t}_{1\beta}|^2}{N_{\text{corr}}}}. \tag{2.5}$$

$\mathcal{T}_1$ values, along with the largest absolute t_{ij}^{ab} amplitudes, were obtained from CCSD(T)/cc-pVTZ computations; the largest CASSCF reference coefficients C_0 were also considered (see Table 2.3 in Sect. 2.7). For CASSCF computations, a full valence active space was selected for species with less than five heavy atoms (i.e., C, N, O). For all other systems, a full valence energy calculation was computationally intractable and a large active space of 20 electrons distributed in 14 orbitals was used. These computations were not utilized for energy predictions.

CASSCF computations were performed using MOLPRO, version 2010.1.[121] IRC computations were performed using GAMESS version May 1, 2013 R1.[122,123] All other computations were performed using CFOUR, version 1.0.[124] The CCSDT and CCSDT(Q) energies were computed using the string-based quantum chemistry code of Kállay (MRCC),[125–127] as interfaced with CFOUR.

2.4 Results and Discussion

A summary of our results is presented in Fig. 2.2, where the overall reaction coordinate is plotted against relative enthalpies at 0 K ($\Delta H_{0\text{K}}$). Tables 2.1 and 2.2 present the incremented focal point extrapolations and corrections used to determine these relative enthalpies. Each energy has a suggested accuracy of ± 1 kcal mol^{-1}, with the exception of **TS3** (*vide infra*). In the FPA tables, there are clear convergences with increasing levels of electron correlation, which instills confidence in the accuracy of the final values. Optimized structures of interest, computed at the CCSD(T)/cc-pVTZ level of theory, are detailed in Figs. 2.3, 2.4, 2.6, and

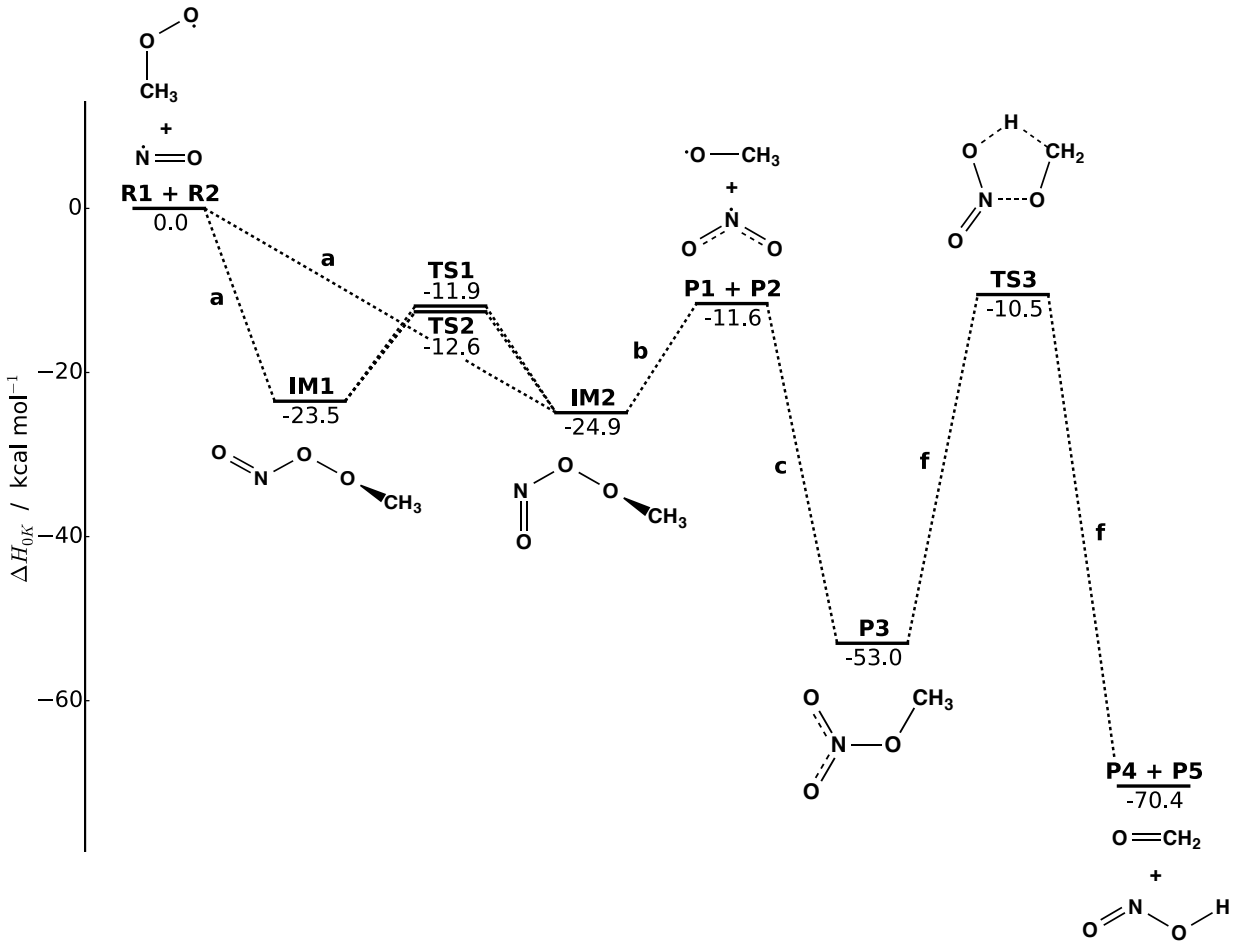

Figure 2.2: Energy profile of the CH_3O_2 + NO reaction system. **TS1** and **TS2** are saddle points corresponding to inward and outward rotations of the OONO dihedral, respectively. Processes **a**, **b**, **c**, and **f** are given in Fig. 2.1.

2.7. All harmonic vibrational frequencies are reported in Sect. 2.8.

In reaction **a** (Fig. 2.1), CH_3O_2 (**R1**) combines with NO (**R2**) in a barrierless process to produce two conformers of CH_3OONO; these are the *trans*-perp (**IM1**, Fig. 2.3) and *cis*-perp (**IM2**, Fig. 2.3) structures. As expected, this radical recombination is exothermic: –23.5 kcal mol^{-1} to **IM1** and –24.9 kcal mol^{-1} to **IM2** (see Table 2.1, parts A and B, respectively). The slight energetic preference for **IM2** results from weak attraction between the terminal

Table 2.1: Incremented focal point tables for the given reactions. The extrapolation scheme and corrections are defined in Sec. 2.3.

A. *trans*-perp CH_3OONO (**IM1**) relative to CH_3O_2 + NO (**R1** + **R2**).

Basis set	ΔE_e[HF]	$+\delta$[MP2]	$+\delta$[CCSD]	$+\delta$[CCSD(T)]	$+\delta$[CCSDT]	$+\delta$[CCSDT(Q)]	ΔE_e[CCSDT(Q)]
cc-pVDZ	+20.98	–49.34	+14.42	–4.99	+0.45	–0.83	[–19.31]
cc-pVTZ	+19.91	–53.90	+16.95	–5.99	[+0.45]	[–0.83]	[–23.40]
cc-pVQZ	+20.10	–55.90	+17.83	–6.20	[+0.45]	[–0.83]	[–24.56]
cc-pV5Z	+20.14	–56.82	+18.22	–6.28	[+0.45]	[–0.83]	[–25.13]
CBS limit	[+20.15]	[–57.79]	[+18.62]	[–6.37]	[+0.45]	[–0.83]	[**–25.77**]

$$\Delta H_{0K} = \Delta E_e + \Delta_{ZPVE} + \Delta_{core} + \Delta_{DBOC} + \Delta_{rel}$$
$$= -25.77 + 2.41 + 0.06 - 0.19 + 0.03 = \mathbf{-23.46\ kcal\ mol^{-1}}$$

B. *cis*-perp CH_3OONO (**IM2**) relative to CH_3O_2 + NO (**R1** + **R2**).

cc-pVDZ	+20.53	–51.73	+15.67	–5.62	+0.51	–0.93	[–21.58]
cc-pVTZ	+20.27	–56.42	+18.16	–6.69	[+0.51]	[–0.93]	[–25.10]
cc-pVQZ	+20.68	–58.47	+19.00	–6.93	[+0.51]	[–0.93]	[–26.14]
cc-pV5Z	+20.78	–59.42	+19.37	–7.01	[+0.51]	[–0.93]	[–26.70]
CBS limit	[+20.82]	[–60.41]	[+19.76]	[–7.10]	[+0.51]	[–0.93]	[**–27.36**]

$$\Delta H_{0K} = -27.36 + 2.51 + 0.07 - 0.19 + 0.02 = \mathbf{-24.95\ kcal\ mol^{-1}}$$

C. **TS1** relative to CH_3O_2 + NO (**R1** + **R2**).

cc-pVDZ	+35.10	–52.95	+15.04	–5.43	+0.66	–0.84	[–8.42]
cc-pVTZ	+35.33	–57.96	+18.00	–6.56	[+0.66]	[–0.84]	[–11.37]
cc-pVQZ	+35.68	–59.98	+18.98	–6.84	[+0.66]	[–0.84]	[–12.35]
cc-pV5Z	+35.76	–60.94	+19.41	–6.95	[+0.66]	[–0.84]	[–12.89]
CBS limit	[+35.78]	[–61.93]	[+19.85]	[–7.05]	[+0.66]	[–0.84]	[**–13.53**]

$$\Delta H_{0K} = -13.53 + 1.69 + 0.13 - 0.18 - 0.01 = \mathbf{-11.90\ kcal\ mol^{-1}}$$

D. **TS2** relative to CH_3O_2 + NO (**R1** + **R2**).

cc-pVDZ	+34.93	–53.25	+15.31	–5.36	+0.64	–0.83	[–8.56]
cc-pVTZ	+34.90	–58.35	+18.33	–6.53	[+0.64]	[–0.83]	[–11.85]
cc-pVQZ	+35.16	–60.41	+19.33	–6.82	[+0.64]	[–0.83]	[–12.94]
cc-pV5Z	+35.21	–61.37	+19.77	–6.93	[+0.64]	[–0.83]	[–13.52]
CBS limit	[+35.22]	[–62.38]	[+20.22]	[–7.05]	[+0.64]	[–0.83]	[**–14.17**]

$$\Delta H_{0K} = -14.17 + 1.65 + 0.12 - 0.18 - 0.01 = \mathbf{-12.60\ kcal\ mol^{-1}}$$

Table 2.2: Incremented focal point tables for the given reactions (continued). The extrapolation scheme and corrections are defined in Sec. 2.3.

A. $CH_3O + NO_2$ (**P1** + **P2**) relative to $CH_3O_2 + NO$ (**R1** + **R2**).

Basis set	ΔE_e[HF]	+δ[MP2]	+δ[CCSD]	+δ[CCSD(T)]	+δ[CCSDT]	+δ[CCSDT(Q)]	ΔE_e[CCSDT(Q)]
cc-pVDZ	+0.34	–19.49	+14.54	–3.39	+0.24	–0.46	[–8.24]
cc-pVTZ	–0.65	–19.19	+14.18	–3.19	[+0.24]	[–0.46]	[–9.09]
cc-pVQZ	–1.08	–19.88	+14.31	–3.20	[+0.24]	[–0.46]	[–10.08]
cc-pV5Z	–1.15	–20.07	+14.40	–3.19	[+0.24]	[–0.46]	[–10.23]
CBS limit	[–1.15]	[–20.27]	[+14.50]	[–3.18]	[+0.24]	[–0.46]	[**–10.33**]

$$\Delta H_{0K} = \Delta E_e + \Delta_{ZPVE} + \Delta_{core} + \Delta_{DBOC} + \Delta_{rel}$$
$$= -10.33 - 1.22 - 0.20 + 0^a + 0.12 = \mathbf{-11.63\ kcal\ mol^{-1}}$$

B. CH_3ONO_2 (**P3**) relative to $CH_3O_2 + NO$ (**R1** + **R2**).

cc-pVDZ	–10.38	–55.48	+23.46	–5.53	+0.93	–0.64	[–47.65]
cc-pVTZ	–12.66	–60.06	+25.08	–6.27	[+0.93]	[–0.64]	[–53.62]
cc-pVQZ	–12.84	–62.69	+25.71	–6.45	[+0.93]	[–0.64]	[–55.99]
cc-pV5Z	–12.80	–63.58	+25.99	–6.50	[+0.93]	[–0.64]	[–56.59]
CBS limit	[–12.74]	[–64.51]	[+26.28]	[–6.54]	[+0.93]	[–0.64]	[**–57.22**]

$$\Delta H_{0K} = -57.22 + 4.49 - 0.39 - 0.22 + 0.30 = \mathbf{-53.03\ kcal\ mol^{-1}}$$

C. **TS3** relative to $CH_3O_2 + NO$ (**R1** + **R2**).

cc-pVDZ	+63.05	–82.56	+28.37	–11.48	+1.06	–2.34	[–3.90]
cc-pVTZ	+63.80	–89.00	+32.38	–13.08	[+1.06]	[–2.34]	[–7.17]
cc-pVQZ	+63.63	–91.70	+33.62	–13.42	[+1.06]	[–2.34]	[–9.15]
cc-pV5Z	+63.67	–92.57	+34.14	–13.51	[+1.06]	[–2.34]	[–9.55]
CBS limit	[+63.72]	[–93.49]	[+34.68]	[–13.60]	[+1.06]	[–2.34]	[**–9.96**]

$$\Delta H_{0K} = -9.96 - 0.39 - 0.23 - 0.10 + 0.17 = \mathbf{-10.52\ kcal\ mol^{-1}}$$

D. CH_2O + *trans*-HONO (**P4** + **P5**) relative to $CH_3O_2 + NO$ (**R1** + **R2**).

cc-pVDZ	–34.12	–40.58	+14.93	–3.06	+0.29	–0.43	[–62.99]
cc-pVTZ	–36.21	–44.06	+17.14	–3.66	[+0.29]	[–0.43]	[–66.93]
cc-pVQZ	–36.97	–46.06	+18.04	–3.75	[+0.29]	[–0.43]	[–68.89]
cc-pV5Z	–37.08	–46.91	+18.51	–3.78	[+0.29]	[–0.43]	[–69.40]
CBS limit	[–37.09]	[–47.79]	[+19.01]	[–3.80]	[+0.29]	[–0.43]	[**–69.81**]

$$\Delta H_{0K} = -69.81 - 0.32 - 0.13 - 0.19 + 0.11 = \mathbf{-70.35\ kcal\ mol^{-1}}$$

[a] Δ_{DBOC} omitted. See text.

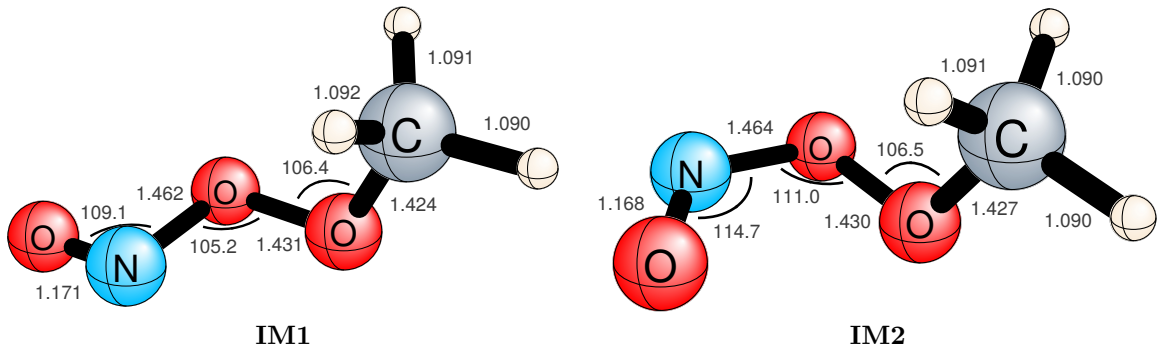

Figure 2.3: Selected geometric parameters in Ångströms and degrees computed at the CCSD(T)/cc-pVTZ level of theory. Both structures possess C_1 point group symmetry.

oxygen atom and the oxygen atom adjacent to the methyl group – an analogous effect is observed in the *cis* and *trans* conformers of the peroxynitrite anion ($OONO^-$).[128] The ONO angles for **IM1** and **IM2** are 109.1° and 114.7°, respectively, which are closer to the roughly 100° value observed for the first excited state of free NO_2 ($^2B_2$) than to that of the $^2A_1$ ground state (134.2°) – see Saeh and Stanton[115] for relevant theoretical literature on the $^2B_2$ state. **IM1** and **IM2** are connected by rotation about the OONO dihedral angle, and there exist two nonequivalent saddle points for rotation: inward rotation (**TS1**, Fig. 2.4) and outward rotation (**TS2**, Fig. 2.4), with the latter being slightly lower in energy (11.6 vs. 10.9 kcal mol^{-1}, see Table 2.1, parts C and D, respectively).

From CH_3OONO, two subsequent pathways exist: reaction **b** and reaction **e**. We first consider the dissociation of **IM2** into CH_3O + NO_2 (**P1** + **P2**), i.e., reaction **b**. At the CCSD(T)/cc-pVTZ level of theory, there are two candidate saddle points for this process, **SP1** and **SP2** (see Fig. 2.8 in Sect. 2.8). These structures appear to lie along the reaction path† corresponding to homolytic OO bond cleavage and a relaxation of the ONO angle from

†**SP1** was not verified by IRC computations, as this structure was not found at the MP2/cc-pVTZ level of theory. The evidence that **SP1** lies along the CCSD(T)/cc-pVTZ reaction path is given by Fig. 2.5.

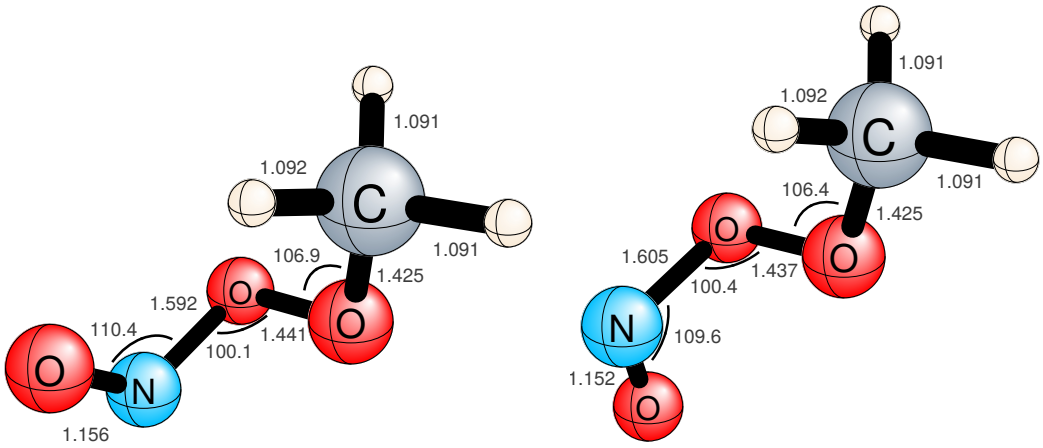

Figure 2.4: Selected geometric parameters in Ångströms and degrees computed at the CCSD(T)/cc-pVTZ level of theory. Both structures possess C_1 point group symmetry.

that observed in **IM2**. The ONO angles in **SP1** and **SP2** are 130.8° and 131.1°, respectively, much closer to the value for ground state NO_2. While these saddle points support the structural conclusions of Zhao and coworkers,[38] we find from constrained optimizations along the reaction path at the CCSD(T)/cc-pVTZ level that a negligible barrier exists. Instead, we approach the $CH_3O + NO_2$ dissociation limit (Fig. 2.5, blue curve).

Analysis of the incremented focal point tables for **SP1** and **SP2** relative to the reactants (see Table 2.5, parts A and B, in Sect. 2.8) provides further evidence for the poor CCSD(T) description of **IM2** $\rightarrow$ **P1** + **P2** dissociation. Table 2.5, parts A and B, displays very slow convergences for **SP1** and **SP2**, suggesting that molecular properties for these systems are not described reliably even at the CCSDT(Q)/CBS level of theory. The large additive corrections from the CCSDT(Q)/cc-pVDZ energies imply that the perturbative treatment of excitation is more sensitive to the choice of reference determinant than are energies at full excitations. This is also the reason that CCSD(T) has been observed to characterize

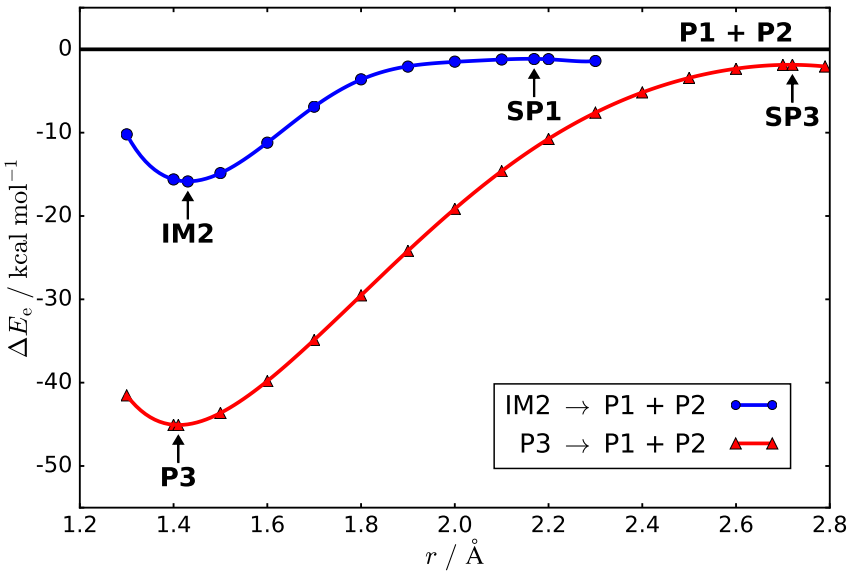

Figure 2.5: Constrained optimization curves for the dissociation of *cis*-perp CH_3OONO (**IM2**; blue curve) and CH_3ONO_2 (**P3**; red curve) into $CH_3O + NO_2$ (**P1** + **P2**; dissociation limit denoted by black line). **SP1** corresponds to the candidate saddle point along the blue curve, and **SP3** corresponds to the candidate saddle point along the red curve (**SP2** also corresponds to the **IM2** $\rightarrow$ **P1** + **P2** dissociation, but does not appear along the blue minimum energy path depicted above). These results are from the CCSD(T)/cc-pVTZ level of theory.

"instability volcanoes" in the NO_2 system even more poorly than CCSD (see above and Refs. 115, 116, 118). Arenas and coworkers[42] optimized a conical intersection in the vicinity of this reaction path, which caused warping of the ground state PES. This finding, coupled with the results of our constrained optimizations and FPA analyses, suggests that these saddle points are artifacts of the single-reference CCSD(T) method failing to accurately describe the reaction path in the vicinity of an excited state PES. We therefore conclude that the homolytic dissociation of **IM2** $\rightarrow$ **P1** + **P2** is a barrierless process.

At the dissociation limit, the two products of reaction **b** (**P1** + **P2**) exist 13.3 kcal mol^{-1} above **IM2** and 11.6 kcal mol^{-1} below the initial reactants (**R1** + **R2**). Note that we have eliminated the anomalously large Δ_{DBOC} energy correction (0.9 kcal mol^{-1}) from Table 2.2,

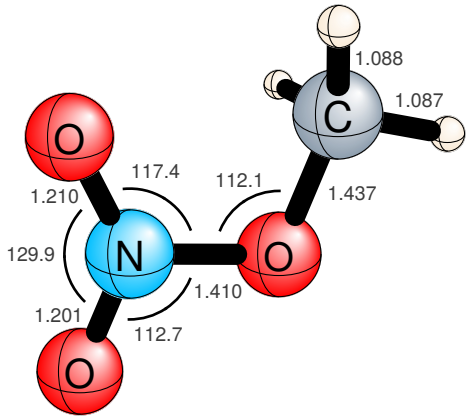

P3

Figure 2.6: Selected geometric parameters in Ångströms and degrees at the CCSD(T)/cc-pVTZ level of theory. This structure possesses C_s point group symmetry (where the σ_h plane contains all C, N, and O atoms, and the H atom on the far right).

Part A. This unphysical result is due to the well-established conical intersection between the $\tilde{X}\ ^2A_1$ and $\tilde{A}\ ^2B_2$ Born-Oppenheimer surfaces of NO_2. Indeed, this conical intersection is closely related to the issues encountered with the dissociation path discussed above.

Regarding reaction **e** – the isomerization of CH_3OONO to methyl nitrate (CH_3ONO_2, **P3**) – we were unable to locate a transition state for direct isomerization starting from either **IM1** or **IM2**. Our attempts to optimize the appropriate species at the CCSD(T) level of theory yielded structures corresponding to OO or NO bond cleavage, in contrast to previous reports at the DFT and MP2 levels.[35,37–41] As a result, we suggest that **P3** is formed through a two-step process involving dissociation of **IM2** (reaction **b**) followed by radical recombination (reaction **c**). The predominance of this reaction path is bolstered by the relative weakness of the OO bond in **IM2** (13.3 kcal mol^{-1}) – the OO bond energy in hydrogen peroxide is 49.2 kcal mol^{-1} by comparison (see Table 2.6 in Sect. 2.8) – and the large exothermic driving force (–41.4 kcal mol^{-1}, see Table 2.2, part B) to **P3** (Fig. 2.6).

We did locate a saddle point, **SP3**, for **P1** + **P2** → **P3** recombination (reaction **c**), but

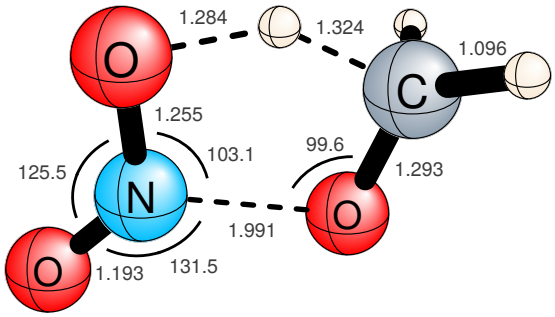

TS3

Figure 2.7: Selected geometric parameters in Ångströms and degrees at the CCSD(T)/cc-pVTZ level of theory. This structure possesses C_s point group symmetry (where the σ_h plane contains all C, N, and O atoms, and the H atom being transferred to the ONO moiety).

again this structure was positioned at the dissociation limit. The geometric parameters of **SP3** are given in Fig. 2.9 in Sect. 2.8. As with **SP1** and **SP2**, structure **SP3** corresponds to homolytic OO bond cleavage, and CCSD(T)/cc-pVTZ constrained optimizations along the reaction path appear to approach the dissociation limit, presenting a negligible barrier (Fig. 2.5, red curve). As expected, and for the same reasons provided in our discussion of **SP1** and **SP2**, the FPA fails to properly describe **SP3** even at CCSDT(Q)/CBS (see Table 2.5, part C, in Sect. 2.8).

As shown in Fig. 2.1, there is another possible channel for **P1** + **P2**, through reaction **d**. We were unable to locate a transition state for this direct H-atom abstraction; our finding is consistent with previous attempts to probe this mechanism.[40] Therefore, dissociation of **P3** to CH_2O (**P4**) and *trans*-HONO (**P5**) is the final reaction considered here (reaction **f**). The transition state for this process, **TS3**, is depicted in Fig. 2.7. Although this structure is a bond-breaking transition state, like the saddle points discussed above, it is better described by the FPA (see Table 2.2, part C), since the two species being formed are closed-shell and the interactions are at closer range. We find the barrier for **TS3** to be 42.5 kcal mol^{-1}, but

this value may require additional scrutiny due to the slow convergence to the CBS limit. However, the CCSDT(Q)/cc-pVDZ additive correction to the final value for **TS3** is smaller (–2.3 kcal mol^{-1}) than those found for **SP1**, **SP2**, and **SP3** (–8.0 kcal mol^{-1}, –8.5 kcal mol^{-1}, and –9.2 kcal mol^{-1}, respectively). Extending the incremented FPA tables to the (currently) computationally intractable CCSDTQ or CCSDTQ(P) methods may allow for a more accurate description of **TS3** by capturing additional multireference character. We note that the transition-state energy for **TS3** may be reduced via interaction with another atmospheric compound,[129–131] such as through double hydrogen transfer, but the entropic penalty may be non-negligible in those cases. The overall reaction energy for **P3** $\rightarrow$ **P4** + **P5** is –17.3 kcal mol^{-1}, with the products placed –70.4 kcal mol^{-1} below the initial reactants **R1** + **R2** (see Table 2.2, part B).

2.5 Conclusions

A high-level theoretical analysis of the CH_3O_2 + NO reaction system is presented. From computations at the CBS limit of CCSDT(Q), we find that the recombination of CH_3O_2 + NO yields two conformers of CH_3OONO (**IM1** and **IM2**) that lie -24 and -25 kcal mol^{-1} below the reactants, respectively. Interconversion between these conformers is possible via two distinct transition states (**TS1** and **TS2**) corresponding to inward and outward rotation of the OONO dihedral. From CH_3OONO, CH_3O and NO_2 may be realized from dissociation of the OO bond – this process is barrierless; we find two candidate transition state structures at the dissociation limit, but they appear from warping of the PES due to a low-lying excited state surface. Methyl nitrate, CH_3ONO_2, is furnished though the combination of CH_3O and NO_2, a process that is exothermic by –41 kcal mol^{-1}. A transition state for direct isomerization from CH_3OONO to CH_3ONO_2 – without dissociation then recombination – could not be obtained at the CCSD(T)/cc-pVTZ level of theory despite previous reports of a candidate structure optimized using DFT and MP2. CH_2O + HONO may be obtained

from CH_3ONO_2 via **TS3**; we find a significant barrier to this process (43 kcal mol^{-1}), likely increasing the lifetime of CH_3ONO_2 in the troposphere. Future characterizations of this critical reaction system will require yet higher level methodologies and explorations of the conical intersections induced by the ONO moiety.

2.6 Acknowledgments

A. M. L. gratefully acknowledges helpful discussions with Dr. Justin M. Turney and Andreas V. Copan. This research is supported by the Department of Energy, Office of Basic Energy Sciences (Grant No. DE-FG02-97-ER14748).

2.7 Appendix: Analysis of Multireference Character

For all compounds, the suitability of employing a single reference determinant was assessed via the $\mathcal{T}_1$ diagnostic (see Sec. 2.3). For closed-shell species, a value of larger than 0.02 has been proposed as an indication of possible multireference character.[119] For open-shell species, this cutoff is not as rigorous, because large orbital-relaxation effects typically yield higher $\mathcal{T}_1$ values.[132] Table 2.3 gives $\mathcal{T}_1$ values, along with the largest $|t_{ij}^{ab}|$ values, and the C_0 reference coefficient for each of the species considered in this research.

By far, **SP1**, **SP2**, and **SP3** have the largest $\mathcal{T}_1$ values of the closed-shell species considered (0.061, 0.059, and 0.054, respectively). **TS3** has a $\mathcal{T}_1$ value of 0.037. To provide further evidence for the multireference character of these CCSD(T)/cc-pVTZ stationary points, and to confirm the single-reference character of the open-shell species, we also present the largest $|t_{ij}^{ab}|$ values obtained for each system. Once again, **SP1**, **SP2**, and **SP3** have the largest values (0.30, 0.32, and 0.40, respectively). **TS3** has the next highest value (0.12), slightly above that of NO (0.11), the highest of the remaining species. The C_0 coefficients for the CASSCF calculations described in Sec. 2.3 are also the lowest of the species considered for

Table 2.3: Diagnostics for stationary points optimized at CCSD(T)/cc-pVTZ. $\mathcal{T}_1$, $|t_{ij}^{ab}|$, and C_0 are defined in Sec. 2.3.

	$\mathcal{T}_1$	largest $\lvert t_{ij}^{ab}\rvert$	C_0
CH_3O_2 (**R1**)	0.045	0.04	0.956
NO (**R2**)	0.042	0.11	0.968
trans-perp CH_3OONO (**IM1**)	0.029	0.06	0.947
cis-perp CH_3OONO (**IM2**)	0.030	0.06	0.936
TS1	0.025	0.07	0.930
TS2	0.025	0.07	0.930
SP1	0.061	0.30	0.795
SP2	0.059	0.32	0.786
CH_3O (**P1**)	0.025	0.03	0.975
NO_2 (**P2**)	0.034	0.09	0.945
SP3	0.054	0.40	0.741
CH_3ONO_2 (**P3**)	0.025	0.10	0.960
TS3	0.037	0.12	0.924
CH_2O (**P4**)	0.022	0.11	0.968
trans-HONO (**P5**)	0.030	0.08	0.949

SP1, **SP2**, and **SP3** (0.795, 0.786, and 0.741, describing only 63.2%, 61.8%, and 54.8% of the total wavefunction, respectively). The dominant reference for **TS3** has a coefficient of 0.924, describing 85.4% of the total wavefunction.

2.8 Supplementary Material

A. Candidate saddle point structures

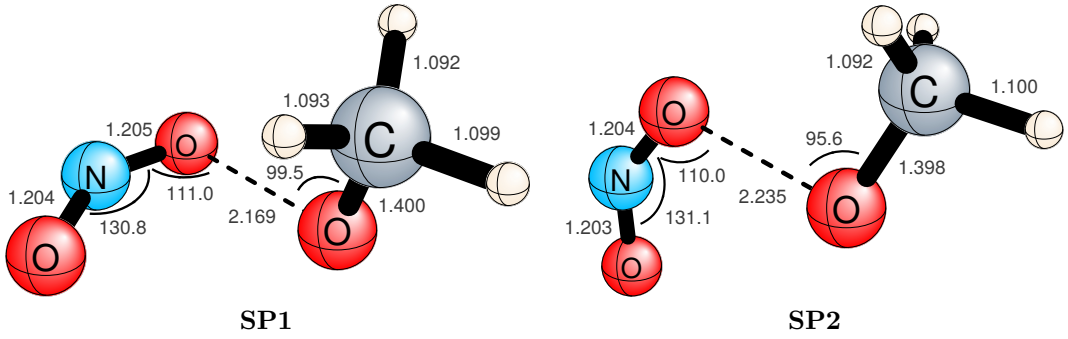

Figure 2.8: Selected geometric parameters in Ångströms and degrees computed at the CCSD(T)/cc-pVTZ level of theory. **SP1** (left) possesses C_1 point group symmetry. **SP2** (right) possesses C_s point group symmetry (where the σ_h plane contains all C, N, and O atoms, and the H atom on the far right).

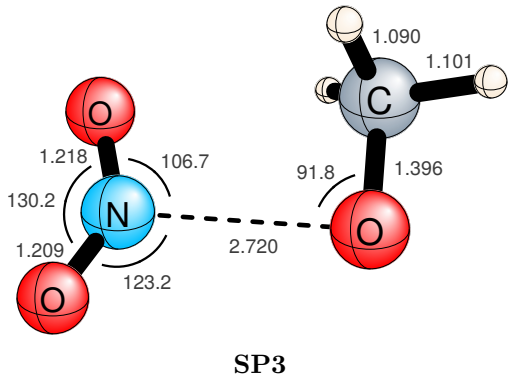

Figure 2.9: Selected geometric parameters in Ångströms and degrees at the CCSD(T)/cc-pVTZ level of theory. This structure possesses C_s point group symmetry (where the σ_h plane contains all C, N, and O atoms, and the H atom on the far right).

B. Supplementary tables

Table 2.4: Anomalous CCSD(T)/cc-pVTZ harmonic vibrational frequencies for UHF and ROHF references compared to anharmonic values from experiment. Frequencies are reported in cm^{-1}.

Molecule	Mode	UHF	ROHF	Experiment
NO	ω_e	2123	1903	1904[a]
NO_2	ω_3	2308	1680	1634[b]

[a] From Ref. 133.

[b] From Ref. 134.

Table 2.5: Incremented focal point tables for the given candidate saddle points relative to CH_3O_2 + NO (**R1** + **R2**). The extrapolation scheme and corrections are defined in Sec. 2.3.

A. **SP1**.

Basis set	ΔE_e[HF]	$+\delta$[MP2]	$+\delta$[CCSD]	$+\delta$[CCSD(T)]	$+\delta$[CCSDT]	$+\delta$[CCSDT(Q)]	ΔE_e[CCSDT(Q)]
cc-pVDZ	+88.76	–100.50	+27.40	–26.47	+3.51	–8.02	[–15.32]
cc-pVTZ	+90.02	–105.67	+33.29	–27.63	[+3.51]	[–8.02]	[–14.50]
cc-pVQZ	+89.90	–107.72	+34.93	–27.93	[+3.51]	[–8.02]	[–15.33]
cc-pV5Z	+89.91	–108.49	+35.58	–28.06	[+3.51]	[–8.02]	[–15.56]
CBS limit	[+89.93]	[–109.30]	[+36.27]	[–28.19]	[+3.51]	[–8.02]	[**–15.79**]

$$\Delta H_{0K} = \Delta E_e + \Delta_{ZPVE} + \Delta_{core} + \Delta_{DBOC} + \Delta_{rel}$$
$$= -15.79 + 0.75 + 0.18 - 0.15 + 0.08 = \mathbf{-14.93\ kcal\ mol^{-1}}$$

B. **SP2**.

Basis set	ΔE_e[HF]	$+\delta$[MP2]	$+\delta$[CCSD]	$+\delta$[CCSD(T)]	$+\delta$[CCSDT]	$+\delta$[CCSDT(Q)]	ΔE_e[CCSDT(Q)]
cc-pVDZ	+93.64	–106.05	+30.00	–28.46	+3.85	–8.50	[–15.52]
cc-pVTZ	+94.48	–111.16	+36.21	–29.48	[+3.85]	[–8.50]	[–14.59]
cc-pVQZ	+94.18	–113.22	+37.98	–29.74	[+3.85]	[–8.50]	[–15.45]
cc-pV5Z	+94.10	–113.98	+38.66	–29.85	[+3.85]	[–8.50]	[–15.73]
CBS limit	[+94.07]	[–114.78]	[+39.37]	[–29.98]	[+3.85]	[–8.50]	[**–15.97**]

$$\Delta H_{0K} = -15.97 + 0.61 + 0.21 - 0.14 + 0.09 = \mathbf{-15.19\ kcal\ mol^{-1}}$$

C. **SP3**.

Basis set	ΔE_e[HF]	$+\delta$[MP2]	$+\delta$[CCSD]	$+\delta$[CCSD(T)]	$+\delta$[CCSDT]	$+\delta$[CCSDT(Q)]	ΔE_e[CCSDT(Q)]
cc-pVDZ	+111.47	–126.82	+39.81	–36.95	+6.31	–9.24	[–15.42]
cc-pVTZ	+110.64	–129.52	+45.70	–37.49	[+6.31]	[–9.24]	[–13.60]
cc-pVQZ	+110.14	–130.94	+47.43	–37.60	[+6.31]	[–9.24]	[–13.89]
cc-pV5Z	+109.90	–131.39	+48.08	–37.64	[+6.31]	[–9.24]	[–13.99]
CBS limit	[+109.76]	[–131.86]	[+48.75]	[–37.69]	[+6.31]	[–9.24]	[**–13.97**]

$$\Delta H_{0K} = -13.97 - 0.22 + 0.42 - 0.14 + 0.11 = \mathbf{-13.81\ kcal\ mol^{-1}}$$

Table 2.6: Incremented focal point table for 2OH relative to HOOH. The extrapolation scheme and corrections are defined in Sec. 2.3.

Basis set	ΔE_e[HF]	$+\delta$[MP2]	$+\delta$[CCSD]	$+\delta$[CCSD(T)]	$+\delta$[CCSDT]	$+\delta$[CCSDT(Q)]	ΔE_e[CCSDT(Q)]
cc-pVDZ	–2.55	+55.76	–9.61	+3.64	–0.07	+0.59	[+47.76]
cc-pVTZ	–1.91	+61.49	–12.65	+5.25	[–0.07]	[+0.59]	[+52.71]
cc-pVQZ	–2.52	+63.59	–13.32	+5.55	[–0.07]	[+0.59]	[+53.82]
cc-pV5Z	–2.76	+64.46	–13.56	+5.66	[–0.07]	[+0.59]	[+54.33]
CBS limit	[–2.88]	[+65.38]	[–13.81]	[+5.77]	[–0.07]	[+0.59]	[**+54.98**]

$$\Delta H_{0K} = \Delta E_e + \Delta_{ZPVE} + \Delta_{core} + \Delta_{DBOC} + \Delta_{rel}$$
$$= 54.98 - 5.96 + 0.17 + 0.10 - 0.13 = \mathbf{49.16\ kcal\ mol^{-1}}$$

Chapter 3

Ethylperoxy Radical: Approaching Spectroscopic Accuracy via Coupled-Cluster Theory*

*A. M. Launder, J. M. Turney, J. Agarwal, and H. F. Schaefer.
To be submitted to *Phys. Chem. Chem. Phys.*

3.1 Abstract

Interest in peroxy radicals derives from their central role in tropospheric and low-temperature combustion processes; however, their transient nature limits the scope of possible experimental characterization techniques. As a result, theoretical methods (notably, coupled-cluster theory) have become indispensable in the reliable prediction of properties of such ephemeral open-shell systems. Herein, the $\tilde{X}$ and $\tilde{A}$ state conformers of ethylperoxy radical ($C_2H_5O_2$) have been structurally optimized at the CCSD(T)/ANO2 level of theory. Relative enthalpies at 0 K [including $\tilde{A} \leftarrow \tilde{X}$ transition origins (T_0)] are reported, incorporating CCSD(T) electronic energies extrapolated to the complete basis set limit via the focal point approach. Higher-level computations, employing basis sets as large as cc-pV5Z and post-HF methods up to CCSDT(Q), prove essential in achieving predictions to within 10 cm^{-1} for experimental T_0: we predict 7363 and 7583 cm^{-1} for the *trans* and *gauche* conformers, respectively. Furthermore, predictions of $\tilde{X}$ state fundamental transitions incorporating CCSD(T)/ANO0 anharmonic contributions are given. For each conformer, all 21 modes were characterized, improving upon the 16 modes reported in the experimental literature [including reassignments of the CH_3 umbrella mode (ν_6) and the OO stretching mode (ν_8)].

3.2 Introduction

Peroxy radicals (RO_2) are ubiquitous in the terrestrial atmosphere, where they serve as intermediates in the propagation of photochemical smog.[13,17] The driving mechanism for this is the RO_2 + NO reaction system, which perturbs ambient tropospheric concentrations of principal photochemical smog components (i.e., NO, NO_2, and O_3).[13,18,20,21,135] RO_2 species also participate in the low-temperature oxidation of hydrocarbon fuels[12,13] – a temperature regime defined by the equilibrium of the R + O_2 $\leftrightharpoons$ RO_2 reaction (which, for simple alkylperoxy radicals, favors dissociation at temperatures in excess of 750 K).[13] It follows

that a fundamental understanding of RO_2 compounds and their properties is imperative for a complete description of both low-temperature combustion and smog chemistries. This motivates the desire to pursue accurate characterizations of RO_2 in the gas phase.

Initial attempts to study RO_2 spectroscopically were dominated by investigations of UV electronic transitions, from which data on reaction kinetics may be derived.[136] However, as most RO_2 radicals do not produce clear UV absorption spectra, studying the electronic structure of individual species proved challenging. Worse, many small alkylperoxy radicals produce nearly identical spectra, further complicating matters. This is because the UV absorption correlates to a $\tilde{B}\ ^2A'' \leftarrow \tilde{X}\ ^2A''$ excitation ($\pi \rightarrow \pi^*$ transition), and the resultant $\tilde{B}$ state is dissociative along the C–O and O–O coordinates.[137–139] Manifestations of this transition are present in each alkylperoxy radical, in which a single broad peak originating from the O–O chromophore is observed.[13,18,140]

In the late 1980s, the experimental focus began to shift to the virtually unexplored IR spectra of RO_2. The earliest assignments of vibrational transitions in this region for the simplest alkylperoxy radicals were reported in a series of matrix isolation studies by Snelson and coworkers.[141–145] Further, distinct vibronic structure may be resolved via near IR excitation to the bound $\tilde{A}$ state. $\tilde{A} \leftarrow \tilde{X}$ transitions of several small alkylperoxy radicals were first reported in a 1976 study by Hunziker and Wendt, in which they identified progressions distinctive of an O–O stretching mode.[146] However, these transitions in alkylperoxy radicals are 10^4 to 10^5 times weaker than the $\tilde{B} \leftarrow \tilde{X}$ transition,[139] which obstructed spectroscopic efforts for decades. Recently, though, the $\tilde{A} \leftarrow \tilde{X}$ transition has been extensively addressed by Miller and coworkers via cavity ringdown spectroscopy (CRDS) experiments.[139] The advent of CRDS has permitted unprecedented measurement of such weak excitations by extending the path length of the exciting laser pulse in an optical cavity.[147,148]

Despite these advances, there remain several obstacles to studying RO_2 in the laboratory.[13,18] One impediment is the rapid rates of RO_2 reactions with other compounds, the

products of which are often also highly reactive radical propagators themselves. Additionally, these products commonly arise from multiple reaction channels, further obfuscating experimental work on individual reactions or species. However, such issues may be further aided, if not fully resolved, by cutting-edge computational methodologies. The success of high-accuracy *ab initio* quantum chemical methods [in particular, coupled-cluster (CC) theories] in describing the chemistry of small gas-phase radicals promotes the complementarity of theory and experiment. This synergy is further abetted via the kinetic modeling of global climate chemistry[19] and combustion processes.[12,30] To this end, our group has recently contributed reliable predictions of the spectroscopic properties of the $\tilde{X}$ and $\tilde{A}$ states of the methylperoxy (CH_3O_2),[149–151] acetylperoxy [$CH_3C(O)O_2$],[31] and formylperoxy [$HC(O)O_2$] radicals,[152] as well as the geometries and fundamental vibrational frequencies of ground-state conformers of *n*-propylperoxy radical (*n*-$C_3H_7O_2$).[153] In this research, we address the ethylperoxy radical ($C_2H_5O_2$), furthering understanding of the energetics and spectroscopy of these important systems.

The first vibrational spectrum of $C_2H_5O_2$ was reported by Chettur and Snelson in 1987;[144] it was not until the early 21st century, however, that additional fundamental transitions of $C_2H_5O_2$ were observed.[154,155] Recent CRDS research has further characterized the kinetics and vibronic transitions of the $\tilde{X}$ and $\tilde{A}$ states of $C_2H_5O_2$.[156–162] This level of precision has permitted the determination of conformer-specific properties of $C_2H_5O_2$ ($C_2H_5O_2$ being the smallest alkylperoxy radical with multiple ground state conformeric minima).

The reported fundamental vibrational frequencies and CRDS results provide benchmarks for quantum chemical predictions of $\tilde{X}$ and $\tilde{A}$ properties of RO_2. The equilibrium geometries and formation of $C_2H_5O_2$,[158,163–172] as well as its place in general trends of alkylperoxy radicals,[173–179] have been addressed in the theoretical literature; its relatively small size makes it an ideal candidate for high-level *ab initio* characterization. However, few of these studies (see Refs. 169 and 172) have reported computations using, at minimum, the "gold

standard" of modern electronic structure theory: coupled-cluster theory with single, double, and perturbative triple excitations [CCSD(T)], paired with a valence triple-ζ basis set. In this research, we examine four stationary points in the $C_2H_5O_2$ system: the $\tilde{X}$ and $\tilde{A}$ state *trans* and *gauche* conformers. For each species, we report CCSD(T)/ANO2 equilibrium geometries and harmonic vibrational frequencies, along with CCSD(T)/ANO0 anharmonic corrections for both $\tilde{X}$ state conformers. We additionally provide relative enthalpies at 0 K (ΔH_{0K}) between each pair of minima [including conformeric $\tilde{A} \leftarrow \tilde{X}$ transition origins (T_0)], computed using the focal point approach.

3.3 Theoretical Methods

Optimized equilibrium geometric parameters of $\tilde{X}$ and $\tilde{A}$ state *trans*- and *gauche*-$C_2H_5O_2$ were obtained using coupled-cluster theory with single, double, and perturbative triple excitations [CCSD(T)].[93–98] All atoms were described with the largest NASA Ames atomic natural orbital (ANO) basis sets (i.e., ANO2; H:[4s3p2d1f], Li-Ne:[5s4p3d2f1g]) developed by Almlöf and Taylor.[180] Prior work concluded that the ANO basis sets often provide better predictions of the vibrational frequencies of systems composed of smaller nuclei ($Z < 10$) than do the popular Dunning basis sets of comparable size.[181] Harmonic vibrational frequencies (ω) were obtained at the same level of theory as the geometry optimizations. Optimized structures were subsequently verified as local minima by confirming that each possessed a Hessian index of 0.

Each optimization step was computed using gradients formed via finite difference of energies as implemented in the Psi4 open-source program package.[182] The ω values were further computed via displacements of the converged gradients. These procedures employed a three-point formula that generated up to 43 displacements for the geometry iterations and up to 463 displacements for the harmonic vibrational frequency computations.

For each minimum, a restricted open-shell Hartree–Fock (ROHF) reference wave function

was employed, as this provides a more qualitatively correct picture of the spin-pairing of the electrons than does the unrestricted formalism (UHF). To obtain a suitable reference for the $\tilde{\text{A}}$ *gauche* conformer, which possesses C_1 point group symmetry, the ground-state HOMO and SOMO were rotated by 90° to obtain a starting guess that better approximates the electronic structure of the $\tilde{\text{A}}$ state. For all computations, a "frozen core" approximation was applied, in which the $1s$-like electrons on the C and O atoms were excluded from the post-HF treatment.

Anharmonic corrections ($\delta\nu$) to the CCSD(T)/ANO2 harmonic vibrational frequencies were computed with CCSD(T)/ANO0 (where ANO0 is a truncation of the ANO2 basis sets; H:[$2s1p$], Li-Ne:[$3s2p1d$]); second-order vibrational perturbation theory (VPT2)[183–185] was employed to obtain the $\delta\nu$ values (in which analytic second derivatives were computed at displaced geometries along the normal coordinates).[186] The final values for the fundamental vibrational frequencies (ν) were thus determined by appending the anharmonic corrections to the harmonic vibrational frequencies (i.e., $\nu = \omega + \delta\nu$).

Two Fermi type 2 resonances were identified, and the offending terms were removed from the VPT2 analysis. The resultant deperturbed values, along with the first-order coupling elements of the appropriate modes, were then used to construct an effective 2×2 matrix.[187] The eigenvalues of this matrix give our CCSD(T)/ANO0 predictions for the peaks of the corresponding Fermi resonance dyad. Matrices, eigenvalues, and eigenvectors are presented in Sect. 3.7. This procedure was performed using the PyVPT2 program.[188]

The relative electronic energy (ΔE_e) between *trans*- and *gauche*-$C_2H_5O_2$ was determined using the focal point approach (FPA), a composite extrapolation scheme developed by Allen and coworkers.[100–103] For each conformer, absolute energies computed up to CCSD(T) with Dunning's correlation-consistent basis sets of increasing size (up to cc-pV5Z)[99] and were systematically extrapolated to the complete basis set limit with either a three-parameter exponential extrapolation scheme[104] (for ROHF electronic energies) or a two-parameter power

extrapolation scheme[105] (for post-HF correlation energies).

The relative enthalpies at 0 K ($\Delta H_{0\mathrm{K}}$) were determined as the differences between the extrapolated electronic energies of relevant minima, further refined with the following corrections:

1. Additive corrections, computed with the ANO0 basis sets, were appended for higher excitations in CC theory [up to CCSDT(Q)].[106–108] Due to nonvanishing off-diagonal blocks in the Fock matrix, ROHF-based CCSDT(Q) theory may not be formulated in a manner analogous to UHF-based CCSDT(Q) theory. Two alternative ansätze have been formulated by Kállay and Gauss for use with ROHF references: CCSDT(Q)/A and CCSDT(Q)/B.[108] The more "robust" B variant is used here, following the recommendation of Martin.†

2. Zero-point vibrational energy corrections (Δ_{ZPVE}) were obtained from CCSD(T)/ANO2 frequency computations.

3. Corrections for the frozen core approximation (Δ_{core}) were computed as the difference between all-electron and frozen-core CCSD(T)/cc-pCVQZ energies.‡

4. Corrections for scalar relativistic effects (Δ_{rel}) were computed using the spin-free one-electron exact two-component method (SFX2C-1e), a simplification of the X2C formalism.[190–192] The X2C-1e methods use a Foldy-Wouthuysen transformation[193] of the one-electron Dirac Hamiltonian to obtain a quasirelativistic two-component operator; the scalar spin-free method is then formulated by removing the spin-dependent (vector) terms. The SFX2C-1e computations were performed with the all-electron CCSD(T) method using fully uncontracted cc-pCVTZ basis sets.

†See Ref. 189. The values given by the two variants of ROHF-based CCSDT(Q) theory were almost identical: the relative CCSDT(Q)/A additive corrections were within 2 cm^{-1} of their CCSDT(Q)/B counterparts for each case considered in Table 3.1.

‡See Ref. 109. cc-pCVQZ is a "core-valence" basis set, in that it includes additional functions to describe core electron correlation relative to its valence analog, cc-pVQZ.

To ensure that effects due to static correlation were not degrading the quality of the single determinant approximations, the multireference character of each conformer was assessed by two metrics. First, the largest absolute t_{ij}^{ab} amplitudes that appeared in the CCSD/ANO2 wave functions were considered. These values did not exceed 0.03, less than reference values for HO_2 (0.04) and CH_3 (0.04), open-shell systems that are well-described by single-determinant methodologies. Second, the C_0 values were determined, corresponding to the largest determinantal contribution to the CASSCF(13, 13)/ANO2 wave function. These values were not lower than 0.954 (i.e., the leading determinants comprised at least 91.0% of the given wave function), comparing favorably to the values determined for HO_2 (0.974, which comprised 94.9% of the full-valence CASSCF(13, 9)/ANO2 wave function) and CH_3 (0.983, which comprised 96.7% of the full-valence CASSCF(7, 7)/ANO2 wave function).

Unless indicated below, all computations were performed as implemented in the MOLPRO program package, version 2010.1.[121] Anharmonic corrections were computed using the CFOUR program package, version 1.0.[124] Relativistic corrections were computed using PSI4.[182,194] The CCSDT and CCSDT(Q) energies were computed using the MRCC code developed by Kállay[125–127] (as interfaced with PSI4).

3.4 Results and Discussion

The present findings on the $C_2H_5O_2$ system are reported in three sections: i) we discuss the electronic structure in the context of the equilibrium nuclear framework and the qualitative features of the $\tilde{X}$ and $\tilde{A}$ CCOO torsional potentials; ii) we detail the results of our focal point extrapolations, analyzing patterns of convergence and the reliability of our computed ΔH_{0K} values; and iii) we report anharmonic fundamental frequencies, in some cases modifying previous assignments of the corresponding normal modes.

3.4.1 Equilibrium Geometries

The CCSD(T)/ANO2 equilibrium bond lengths, CCO and COO bond angles, and CCOO dihedrals of the $\tilde{X}$ and $\tilde{A}$ states of $C_2H_5O_2$ are presented in Fig. 3.1. Little change is observed in the bond lengths between the two conformers on the $\tilde{X}$ surface. Apart from the defining CCOO dihedral, the most noteworthy difference between the parameters detailed in Fig. 3.1 is the CCO angle, which is 3.7° greater in the *gauche* conformer (where the CH_3 group responds sterically to the rotation of the OO moiety). This effect is further pronounced on the $\tilde{A}$ surface, in which the CCO angle is 6.8° greater in the *gauche* conformer.

The $\tilde{A} \leftarrow \tilde{X}$ transition involves the excitation of an electron from the HOMO into the SOMO. Both of these orbitals are centered on the OO moiety, with the former correlating to an in-plane π^* orbital, and the latter to an out-of-plane π^* orbital (these MOs are shown in Fig. 10 of Ref. 139). We would thus expect little effect on bond lengths involving exclusively C and H atoms, which change by a maximum of 0.003 Å following excitation. The most noticeable changes occur in the equivalent C–H_d/C–H_e bond lengths of the *trans* conformer, and in the C–H_d and C–C bond lengths of the *gauche* conformer. This is attributed to a similar hyperconjugative effect as that in the CH_3O_2 radical, in which doubly occupying the out-of-plane OO π^* orbital enhances the p character of the out-of-plane C–H bonding.[151] The O–O bond also sees remarkable lengthening (by greater than 0.08 Å in both conformers) when this orbital is doubly occupied. This is consistent with bond distance increases of similar magnitudes found in previous theoretical work on peroxy radicals,[31,151,152] as well as in experiments on HO_2.[195]

To elucidate the qualitative differences in the CCOO torsional potentials on the $\tilde{X}$ and $\tilde{A}$ surfaces, we performed a CCSD(T)/ANO0 constrained optimization scan along the τ(CCOO) coordinate for both electronic states considered (see Fig. 3.2). We first highlight the topographical characteristics of the two potentials, with the barriers on the $\tilde{A}$ surface

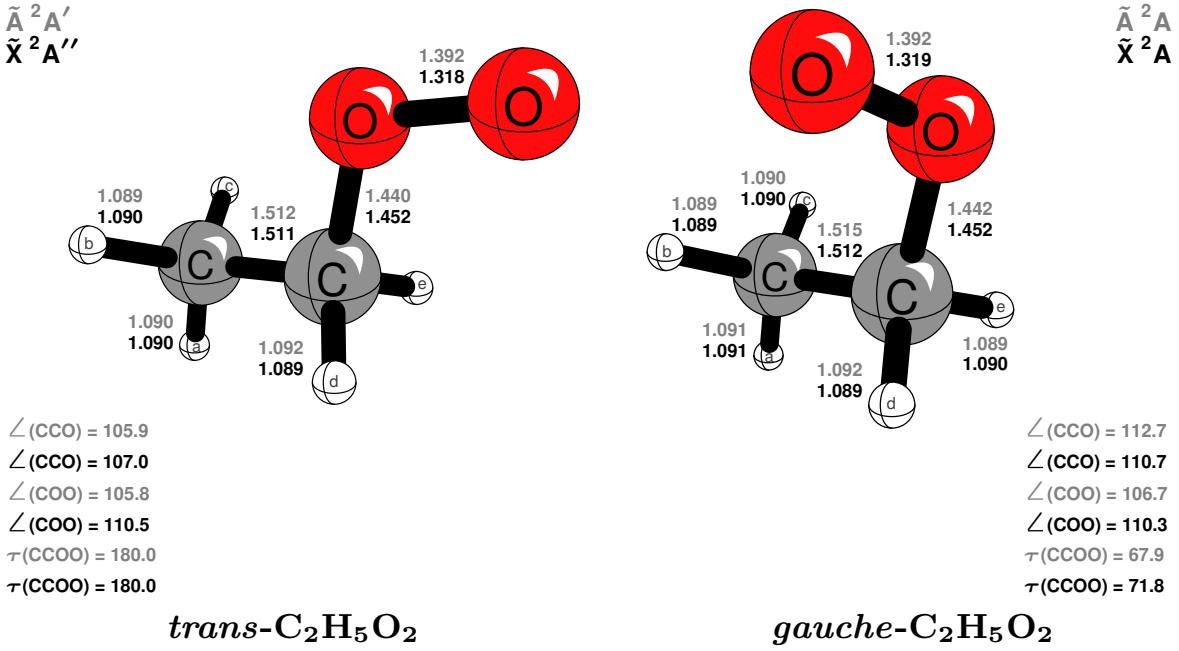

Figure 3.1: Selected equilibrium geometric parameters in Ångströms and degrees of the *trans* and *gauche* conformers of $C_2H_5O_2$ obtained at the CCSD(T)/ANO2 level of theory. Values displayed correspond to minima on the $\tilde{X}$ (in bold) and $\tilde{A}$ (in gray) surfaces. The *trans* conformer possesses C_s point-group symmetry (where the σ_h plane contains all C and O atoms, and the bottommost H atom on the methyl group) and the *gauche* conformers possess C_1 point-group symmetry.

being approximately twice as high as those on the $\tilde{X}$ surface relative to the global minimum. We also note that the conformer corresponding to the global minimum has changed between electronic states: on the $\tilde{X}$ surface, the *gauche* conformer is the global minimum, while on the $\tilde{A}$ surface, the *trans* conformer is the global minimum. As may be seen in Fig. 3.2, the conformer differences in electronic energies ($\Delta E_e^{|g-t|}$) are < 1 kcal mol^{-1} (cf. Sec. 3.4.2). This, coupled with the relatively low barrier to conformeric isomerization, suggests that effectively free CCOO torsion is expected at temperatures observed in the troposphere or low-temperature combustion.

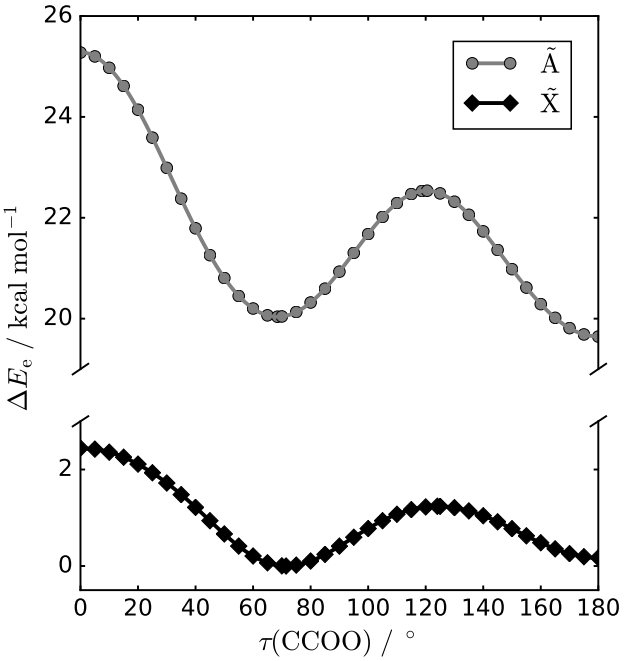

Figure 3.2: Potential curves for rotation about the CCOO dihedral angle of $C_2H_5O_2$ (see Fig. 3.1) on the $\tilde{X}$ (defined by black diamonds) and $\tilde{A}$ (defined by gray circles) surfaces. Individual energy values are derived from CCSD(T)/ANO0 geometry optimizations in which the CCOO dihedral was constrained. All energies are relative to the global minimum on the $\tilde{X}$ surface (in which the nuclear framework corresponds to the equilibrium geometry of the *gauche* conformer).

3.4.2 Focal Point Extrapolations

Relevant incremented focal point extrapolations and corrections are given in Table 3.1, from which we derive highly reliable conformational enthalpy differences at 0 K ($\Delta H_{0K}^{|g-t|}$) and $\tilde{A} \leftarrow \tilde{X}$ transition origins (T_0) of the $C_2H_5O_2$ system. One useful feature of presenting FPA results in this manner is the analysis of convergence patterns. By assessing the quality of convergence of relative corrections to the ROHF ΔE_e across higher levels of correlation computed using a single basis set, we may obtain an idea of the validity of our single-determinant approximation. For all three ΔE_e values considered in the incremented focal

point schemes presented in Table 3.1, we observe a clear convergence pattern. The highest order CCSDT(Q)/B/ANO0 corrections are < 0.1 kcal mol^{-1} (for counterfactual examples of this smooth convergence behavior, see the discussions on spurious saddle points in our research on CH_3O_2 + NO).[135]

We found the $\Delta H_{0K}^{|g-t|}$ to be 44 cm^{-1} on the $\tilde{X}$ surface and 175 cm^{-1} on the $\tilde{A}$ surface (note that the global minima correspond to different conformers on the respective surfaces; see Sec. 3.4.1 above). Due to the similarities in electronic structure between conformers, the relative additive higher-order, core, and relativistic corrections did little to change the CCSD(T)-extrapolated enthalpies: in total, these corrections summed to +2 cm^{-1} for the $\tilde{X}$ state $\Delta H_{0K}^{|g-t|}$ value and –5 cm^{-1} for the $\tilde{A}$ state $\Delta H_{0K}^{|g-t|}$ value.

For the $\tilde{A} \leftarrow \tilde{X}$ T_0 values, we predict values of 7363 and 7583 cm^{-1} for the *trans* and *gauche* cases, respectively. These results compare favorably (within 10 cm^{-1}) with the experimental values determined by Miller and coworkers:[158] 7362(1) and 7592(1) cm^{-1} for the *trans* and *gauche* cases, respectively. However, contrasting with the determination of the $\Delta H_{0K}^{|g-t|}$ values detailed above, we found that the differences in electronic character between the $\tilde{X}$ and $\tilde{A}$ surfaces produce larger relative additive corrections. Most significant are the higher-order CC corrections (i.e., the $+\delta$[CCSDT/ANO0] and $+\delta$[CCSDT(Q)/B/ANO0] corrections; see Table 3.1, Parts B and C), which contribute 46 and 43 cm^{-1} to the final *trans* and *gauche* T_0 values, respectively. These findings underscore the necessity of going beyond CCSD(T) theory when seeking spectroscopic accuracy.

To provide further evidence for the use of the FPA in the accurate determination of RO_2 $\tilde{A} \leftarrow \tilde{X}$ T_0 values, we performed an equivalent analysis on the smaller CH_3O_2 and HO_2 species (see Table 3.4 in Sect. 3.7). For CH_3O_2, we predicted a T_0 value of 7376 cm^{-1}, which is quite close to Jacox's recommended value[196] of 7382.8(5) cm^{-1} (derived from the experimental work performed by Pushkarsky, Zalyubovsky, and Miller).[156] The interested reader is also directed to our previous research on CH_3O_2, which recovers even more of the

Table 3.1: Incremented focal point table for relevant enthalpy differences at 0 K (ΔH_{0K}) for the $C_2H_5O_2$ system. See Sec. 3.3 for nuances of the different theoretical methods, extrapolation schemes, and corrections. All unlabeled values are in cm^{-1}.

A. $\tilde{X}\ ^2A''$ *trans*-$C_2H_5O_2$ relative to $\tilde{X}\ ^2A$ *gauche*-$C_2H_5O_2$.

Basis set	ΔE_e[ROHF]	$+\delta$[RMP2]	$+\delta$[CCSD]	$+\delta$[CCSD(T)]	$+\delta$[CCSDT]	$+\delta$[CCSDT(Q)/B]	ΔE_e[CCSDT(Q)/B]
ANO0[a]	–139	+148	+8	+42	–0	+3	[+63]
cc-pVTZ	–124	+191	+6	+50	[–0]	[+3]	[+126]
cc-pVQZ	–151	+190	+1	+49	[–0]	[+3]	[+91]
cc-pV5Z	–157	+190	–1	+48	[–0]	[+3]	[+84]
CBS limit	[–158]	[+191]	[-3]	[+48]	[–0]	[+3]	**[+81]**

$$\Delta H_{0K} = \Delta E_e + \Delta_{ZPVE} + \Delta_{core} + \Delta_{rel}$$
$$= 81 - 36 - 2 + 0 = \mathbf{44\ cm^{-1}\ (0.13\ kcal\ mol^{-1})}$$

B. $\tilde{A}\ ^2A'$ *trans*-$C_2H_5O_2$ relative to $\tilde{X}\ ^2A''$ *trans*-$C_2H_5O_2$.

ANO0[a]	+4272	+2326	+53	+202	+17	+29	[+6898]
cc-pVTZ	+4477	+2310	+156	+272	[+17]	[+29]	[+7262]
cc-pVQZ	+4515	+2357	+182	+295	[+17]	[+29]	[+7396]
cc-pV5Z	+4517	+2369	+193	+306	[+17]	[+29]	[+7430]
CBS limit	[+4513]	[+2382]	[+204]	[+317]	[+17]	[+29]	**[+7461]**

$$\Delta H_{0K} = 7461 - 116 + 25 - 7 = \mathbf{7363\ cm^{-1}\ (21.05\ kcal\ mol^{-1})}$$

C. $\tilde{A}\ ^2A$ *gauche*-$C_2H_5O_2$ relative to $\tilde{X}\ ^2A$ *gauche*-$C_2H_5O_2$.

ANO0[a]	+4394	+2429	+11	+219	+11	+33	[+7097]
cc-pVTZ	+4636	+2469	+97	+299	[+11]	[+33]	[+7545]
cc-pVQZ	+4668	+2517	+120	+323	[+11]	[+33]	[+7672]
cc-pV5Z	+4667	+2527	+130	+334	[+11]	[+33]	[+7702]
CBS limit	[+4662]	[+2538]	[+140]	[+345]	[+11]	[+33]	**[+7729]**

$$\Delta H_{0K} = 7729 - 163 + 23 - 6 = \mathbf{7583\ cm^{-1}\ (21.68\ kcal\ mol^{-1})}$$

[a] Utilized in computation of additive corrections for higher order excitations (no contribution to extrapolation scheme).

correlation energy via the FPA and provides extensive discussion complementary to that presented here.[151] For HO_2, we determined a T_0 value of 7011 cm^{-1}, compared to Jacox's recommended value[196] of 7029.688 cm^{-1} (derived from the experimental work performed by Fink and Ramsay).[197] All four of the T_0 values that we computed are within 20 cm^{-1} of the representative experimental work, suggesting that T_0 values of RO_2 can be accurately captured using traditional CC theory extrapolated and corrected via the FPA.

3.4.3 Fundamental Vibrational Frequencies

The CCSD(T)/ANO2 harmonic vibrational frequencies (ω) and CCSD(T)/ANO0 anharmonic corrections ($\delta\nu$), summed to provide our final predictions for the fundamental vibrational frequencies (ν), are presented for the $\tilde{X}$ state conformers of $C_2H_5O_2$ in Table 3.2. Each row of values is assigned a normal mode and a qualitative description. The *trans* values are canonically sorted by C_s point group symmetry. Because the *gauche* nuclear framework and electronic structure are so similar to that of the *trans* conformer, we also assign nominal symmetry labels to the normal modes of the *gauche* conformer that correlate to those observed in the *trans* conformer. We additionally list assignments of fundamental transitions determined by previous experimental work. [CCSD(T)/ANO2 harmonic vibrational frequencies and assignments for the $\tilde{A}$ state conformers of $C_2H_5O_2$ are reported in Table 3.3 in Sect. 3.7].

In 1987, Chettur and Snelson[144] first reported peaks corresponding to fundamental transitions of $C_2H_5O_2$ in an Ar matrix isolation study. Two later gas phase studies (Blanksby and coworkers in 2001[154] and Mah and coworkers in 2003[155]) provide the remaining experimental assignments currently found in the literature. Most of the reported values from these three studies agree with transitions presented in this work, as do many of their qualitative descriptions of the normal modes. These considerations lead us to trust in the overall quality of the reported spectra. We will discuss a couple of cases, however, where our results deviate from these analyses. We considered both the numerical agreement to our computed results, as

Table 3.2: Computational predictions for harmonic (ω) and fundamental ($\nu = \omega + \delta\nu$) vibrational frequencies and experimental peak assignments of $\tilde{X}\ ^2A''$ *trans*- and $\tilde{X}\ ^2A$ *gauche*-$C_2H_5O_2$. Computational details are presented in Sec. 3.3. All values are in cm^{-1}.

			trans-$C_2H_5O_2$			*gauche*-$C_2H_5O_2$			Experimental ν		
Mode	Description	Symm.[a]	ω	$\delta\nu$	ν	ω	$\delta\nu$	ν	Ref. 144[b,c]	Ref. 154[d]	Ref. 155[c,d]
ν_1	CH_3 antisym. str.	a'	3136	–148	2988	3135	–149	2986			2988
ν_2	CH_2 sym. str.	a'	3076	–108	2968	3079	–122	2957			2964
ν_3	CH_3 sym. str.	a'	3053	–102	2952	3051	–103	2947			
ν_4	CH_3/CH_2 scissor	a'	1517	–42	1475	1511	–42	1470	1474		
ν_5	CH_3/CH_2 scissor	a'	1506	–41	1464	1494	–40	1455			
ν_6	CH_3 umbrella	a'	1424	–34	1389	1413	–33	1380	1380,[e] 1389		1397
ν_7	CH_2 wag	a'	1383	–34	1349	1383	–34	1348	1351		
ν_8	OO str.	a'	1185	–33	1152	1160	–37	1123	1112	1089(16)	(1050, 1062, 1070)[e]
ν_9	CH_3 rock	a'	1148	–28	1120	1110	–28	1082			1110
ν_{10}	CC str.	a'	1046	–29[f]	1017	1018	–26	992	1009		
ν_{11}	CO str.	a'	866	–19	846	866	–21	845	838		880
ν_{12}	COO bend	a'	507	–7	500	531	–2	529	499		
ν_{13}	CCO bend	a'	309	–3	306	363	–4	359			
ν_{14}	CH_3/CH_2 antisym. str.	a''	3148	–144	3004	3153	–152	3002	3016		2999
ν_{15}	CH_3/CH_2 antisym. str.	a''	3126	–155	2971	3129	–149	2980			
ν_{16}	CH_3 deform.	a''	1494	–25	1469	1490	–42	1448	1451		1448
ν_{17}	CH_2 twist	a''	1283	–38[g]	1245	1312	–36	1276	1242		1283
ν_{18}	CH_2 twist	a''	1162	–23	1139	1205	–29	1175	1136		1173
ν_{19}	CH_3/CH_2 antisym. rock	a''	806	–4	802	802	–9	794	800		
ν_{20}	CH_3 torsion	a''	231	–14	217	234	–20	215		234(9)	
ν_{21}	CCOO torsion	a''	89	–6	83	125	–10	115			

[a] In the case of *gauche*-$C_2H_5O_2$, the symmetry labels correlate with the symmetry of the analogous mode in *trans*-$C_2H_5O_2$.
As the gauche conformer possesses C_1 symmetry, its normal modes are rigorously of a symmetry.
[b] Ar matrix value.
[c] Some values reassigned; see text.
[d] Gas phase value.
[e] Dubious assignment; see text.
[f] Mode affected by Fermi type 2 resonance ($\omega_{10} \approx \omega_{19} + \omega_{20}$); deperturbed value given (see Sect. 3.3).
[g] Mode affected by Fermi type 2 resonance ($\omega_{17} \approx \omega_{10} + \omega_{20}$); deperturbed value given (see Sect. 3.3).

well as the chemical rationale given in prior experimental work, when matching our normal modes to peaks determined spectroscopically. Because the qualitative descriptions in the experimental studies are partially rationalized from computations conducted at less reliable levels of theory, we believe that our analysis serves to complement and correct the literature. As the reported experimental peaks have not been attributed to specific conformers, average deviations (see below) are based on the closest computed conformeric value for the assigned normal mode.

For the majority of peaks reported in the literature, we see remarkable agreement with our computed fundamental values. Comparing between our work and Ref. 144, we found an average deviation of 4 cm^{-1} [where we have excluded the CC stretch (ν_{10}) and one of the CH_2 twists (ν_{17}), modes that are perturbed by Fermi type 2 resonances in the *trans* conformer], and between our work and Ref. 155, we found an average deviation of 8 cm^{-1} [where we have excluded the OO stretch (ν_8); see below]. These values serve to benchmark the quality of our results and provide confidence in our predictions of modes which have not yet been assigned in the experimental literature [namely, the CH_3 symmetric stretch (ν_3), one of the CH_3/CH_2 scissors (ν_5), the CCO bend (ν_{13}), one of the CH_3/CH_2 antisymmetric stretches (ν_{15}), and the CCOO torsion (ν_{21})].

We finish our analysis with discussions of some dubious assignments of the CH_3 umbrella (ν_6) and the OO stretch (ν_8). Starting with ν_6, we note that the lone assignment consisted of a low intensity peak at 1380 cm^{-1} in Chettur and Snelson's work.[144] We found this assignment suspect, as the more intense peak at 1389 cm^{-1} that had also been attributed to $C_2H_5O_2$ showed much clearer depletion following Hg arc irradiation (which the authors ascribed to the decomposition of $C_2H_5O_2$ under these conditions). We therefore assigned this latter peak to ν_6, and remove the former peak from consideration.

Next, we consider ν_8, which we predicted at 1152 and 1123 cm^{-1} for the *trans* and *gauche* conformers, respectively. The egregious discrepancy between our ν_8 values and those

determined by Mah and coworkers lead us to consider their results more carefully. Their study[155] reported three possible peaks as corresponding to the OO stretching mode. These features lie at 1050, 1062, and 1070 cm^{-1}, which differ from our computed fundamental values by more than 50 cm^{-1}. These values are also in poor agreement with the gas phase value of 1089(16) cm^{-1} reported by Blanksby and coworkers.[154] The strong intensity of the three peaks in Mah et al. likely wash out the actual peak corresponding to ν_8, which we suggest lies closer to the value determined in Blanksby et al. Removing the values reported by Mah and coworkers from consideration, we found that our lowest computed value (for the *gauche* conformer) lies 11 cm^{-1} from the Ar matrix peak in Chettur and Snelson's work,[144] and outside of the range of accuracy of the remaining gas phase value by 18 cm^{-1}.

3.5 Conclusions

We report highly reliable coupled-cluster predictions concerning the $\tilde{X}$ and $\tilde{A}$ states of the $C_2H_5O_2$ radical, including CCSD(T) equilibrium geometries and harmonic vibrational frequencies computed with the large NASA Ames ANO basis sets (ANO2). The size and reported reliability of the ANO2 basis sets give us confidence in the unprecedented accuracy of these predictions. We find that changes in bond lengths between corresponding conformers on differing electronic states are consistent with a hyperconjugative effect related to that previously reported in the CH_3O_2 system. Focal point extrapolations calculated using single point energies obtained at these equilibrium geometries predict $\tilde{A} \leftarrow \tilde{X}$ T_0 values of 7363 and 7583 cm^{-1} for the *trans* and *gauche* conformers, respectively, values that match experimental work to within 10 cm^{-1}. We stress the importance of recovering correlation via higher-order CC theory [beyond CCSD(T)] in obtaining this level of accuracy for RO_2 – a claim that we reinforce with determinations of T_0 values for the CH_3O_2 and HO_2 systems at the same level of theory. We additionally employ VPT2 and CCSD(T)/ANO0 computations to determine anharmonic corrections to the CCSD(T)/ANO2 harmonic vibrational frequencies. We use

these results to complement and revise the fundamental assignments present in the literature. Comparison to the most reliable experiments underscores the ability of CC theory to determine molecular properties of RO_2 systems approaching spectroscopic accuracy. On the basis of our findings, we suggest that the methods detailed herein may be readily adapted to larger alkylperoxy radical systems to obtain highly reliable predictions pertinent to future experimental work.

3.6 Acknowledgments

A. M. L. gratefully acknowledges helpful discussions with Prof. Gary E. Douberly and Preston R. Hoobler. This research was supported by the Department of Energy, Office of Basic Energy Sciences (Grant No. DE-SC0015512).

3.7 Supplementary Materials

A. Fermi Type 2 Resonance Data

- Fermi type 2 resonance due to $\omega_{19} + \omega_{20} \approx \omega_{10}$.

  First-order coupling matrix (all values in cm^{-1}):

$$\begin{pmatrix} \tilde{\nu}_{19} + \tilde{\nu}_{20} + \tilde{X}_{19,20} & \frac{\phi_{10,19,20}}{\sqrt{8}} \\ \frac{\phi_{10,19,20}}{\sqrt{8}} & \tilde{\nu}_{10} \end{pmatrix} = \begin{pmatrix} 1033.26 & 8.21 \\ 8.21 & 1016.30 \end{pmatrix}$$

  Eigenvalues of first-order coupling matrix:

$$\lambda_- = 1012.98 \text{ cm}^{-1} \qquad \lambda_+ = 1036.58 \text{ cm}^{-1}$$

Eigenvectors of first-order coupling matrix:

$$v_- = \begin{pmatrix} -0.9269 \\ -0.3752 \end{pmatrix} \qquad v_+ = \begin{pmatrix} 0.3752 \\ -0.9269 \end{pmatrix}$$

- Fermi type 2 resonance due to $\omega_{10} + \omega_{20} \approx \omega_{17}$.

  First-order coupling matrix (all values in cm^{-1}):

$$\begin{pmatrix} \tilde{\nu}_{10} + \tilde{\nu}_{20} + \tilde{X}_{10,20} & \frac{\phi_{10,17,20}}{\sqrt{8}} \\ \frac{\phi_{10,17,20}}{\sqrt{8}} & \tilde{\nu}_{17} \end{pmatrix} = \begin{pmatrix} 1242.14 & -7.93 \\ -7.93 & 1245.10 \end{pmatrix}$$

  Eigenvalues of first-order coupling matrix:

$$\lambda_- = 1235.55 \text{ cm}^{-1} \qquad \lambda_+ = 1251.69 \text{ cm}^{-1}$$

  Eigenvectors of first-order coupling matrix:

$$v_- = \begin{pmatrix} -0.6390 \\ 0.7692 \end{pmatrix} \qquad v_+ = \begin{pmatrix} -0.7692 \\ -0.6390 \end{pmatrix}$$

B. Supplementary Tables

Table 3.3: CCSD(T)/ANO2 predictions for harmonic vibrational frequencies (ω) of $\tilde{A}\ ^2A'$ *trans*- and $\tilde{A}\ ^2A$ *gauche*-$C_2H_5O_2$. All values are in cm^{-1}.

Mode	Description	Symmetry[a]	*trans*-$C_2H_5O_2$	*gauche*-$C_2H_5O_2$
ω_1	CH_3 antisym. str.	a'	3137	3130
ω_2	CH_3 sym. str.	a'	3055	3050
ω_3	CH_2 sym. str.	a'	3044	3056
ω_4	CH_3/CH_2 scissor	a'	1535	1511
ω_5	CH_3/CH_2 scissor	a'	1510	1496
ω_6	CH_3 umbrella	a'	1420	1419
ω_7	CH_2 wag	a'	1391	1388
ω_8	CH_3 rock	a'	1135	1115
ω_9	CC str.	a'	1052	1048
ω_{10}	OO str.	a'	982	946
ω_{11}	CO str.	a'	866	859
ω_{12}	COO bend	a'	437	460
ω_{13}	CCO bend	a'	286	339
ω_{14}	CH_3/CH_2 antisym. str.	a''	3146	3149
ω_{15}	CH_3/CH_2 antisym. str.	a''	3091	3124
ω_{16}	CH_3 deform.	a''	1490	1490
ω_{17}	CH_2 twist	a''	1284	1314
ω_{18}	CH_2 twist	a''	1192	1182
ω_{19}	CH_3/CH_2 antisym. rock	a''	835	803
ω_{20}	CH_3 torsion	a''	236	231
ω_{21}	CCOO torsion	a''	141	131

[a] In the case of *gauche*-$C_2H_5O_2$, the symmetry labels correlate with the symmetry of the analogous mode in *trans*-$C_2H_5O_2$. As the *gauche* conformer possesses C_1 symmetry, its normal modes are rigorously of a symmetry.

Table 3.4: Incremented focal point table for $\tilde{A} \leftarrow \tilde{X}$ transition origins (T_0) for the CH_3O_2 and HO_2 systems. The extrapolation scheme and corrections are defined in Sec. 3.3. All unlabeled values are in cm^{-1}.

A. $\tilde{A}\ ^2A'$ CH_3O_2 relative to $\tilde{X}\ ^2A''$ CH_3O_2.

Basis set	ΔE_e[ROHF]	$+\delta$[RMP2]	$+\delta$[CCSD]	$+\delta$[CCSD(T)]	$+\delta$[CCSDT]	$+\delta$[CCSDT(Q)/B]	ΔE_e[CCSDT(Q)/B]
ANO0[a]	+4251	+2279	+70	+203	+19	+28	[+6850]
cc-pVTZ	+4483	+2289	+173	+280	[+19]	[+28]	[+7273]
cc-pVQZ	+4522	+2338	+201	+304	[+19]	[+28]	[+7411]
cc-pV5Z	+4522	+2350	+212	+315	[+19]	[+28]	[+7445]
CBS limit	[+4518]	[+2362]	[+223]	[+326]	[+19]	[+28]	**[+7476]**

$$T_0 = \Delta E_e + \Delta_{ZPVE} + \Delta_{core} + \Delta_{rel}$$
$$= 7476 - 115 + 22 - 7 = \mathbf{7376\ cm^{-1}}\ \mathbf{(21.09\ kcal\ mol^{-1})}$$

B. $\tilde{A}\ ^2A'$ HO_2 relative to $\tilde{X}\ ^2A''$ HO_2.

ANO0[a]	+4508	+1908	–40	+165	+16	+19	[+6577]
cc-pVTZ	+4762	+1949	+41	+231	[+16]	[+19]	[+7018]
cc-pVQZ	+4796	+1989	+63	+249	[+16]	[+19]	[+7132]
cc-pV5Z	+4795	+1993	+70	+257	[+16]	[+19]	[+7149]
CBS limit	[+4789]	[+1996]	[+77]	[+265]	[+16]	[+19]	**[+7162]**

$$T_0 = 7162 - 155 + 10 - 7 = \mathbf{7011\ cm^{-1}}\ \mathbf{(20.05\ kcal\ mol^{-1})}$$

[a] Utilized in computation of additive corrections for higher order excitations (no contribution to extrapolation scheme).

Chapter 4

Conclusions

We have presented coupled-cluster (CC) investigations into the properties and reactions of the smallest alkylperoxy radicals, CH_3O_2 and $C_2H_5O_2$, studies which provide archetypal examples of key peroxy radical (RO_2) chemistry. We first established the importance of RO_2 species in combustion and tropospheric chemistries, and motivated the use of CC theory in providing reliable descriptions of the molecular properties of these radicals. In Chapter 2, we revised prior predictions of the CH_3O_2 + NO reaction mechanism. We determined that this reaction proceeds through a pair of CH_3OONO intermediates, which then dissociate in a barrierless process to CH_3O + NO_2 (products which are 12 kcal mol^{-1} lower in energy than the initial reactants). We further clarified that CH_3ONO_2 is formed exclusively via recombination of these products – a process which is exothermic by 41 kcal mol^{-1}. Because its second dissociation channel (that which leads to CH_2O + HONO) has a barrier of 43 kcal mol^{-1}, we surmised that CH_3ONO_2 is likely a long-lived tropospheric sink for NO_x pollutants. In Chapter 3, we found that properties of $C_2H_5O_2$ logically follow from trends established by prior work on alkylperoxy radicals (for example, a similar hyperconjugative effect to that observed in CH_3O_2 was predicted in the equilibrium geometries of the $C_2H_5O_2$ conformers). Our predicted $\tilde{A} \leftarrow \tilde{X}$ transition origins were 7363 and 7583 cm^{-1} for the *trans* and *gauche* conformers, respectively – these values fall within 10 cm^{-1} of those determined

by experiment. Additionally, we revised assignments of $\tilde{X}$ state fundamental transitions, augmenting the experimental literature.

When relevant, extensive comparisons and references to experiment were included, substantiating the use of CC theory for RO_2 species. The work presented herein is thus another piece in the massive body of evidence for the CC-theoretical description of open-shell chemical compounds. Further work is needed to extend these findings to more difficult reaction systems. High-level multireference investigations are necessary to describe some of the long-standing problems that remain to be solved in RO_2 reaction systems. The prevalence of ubiquitous and troublesome conical intersections, along with the multireference issues associated with small, atmospherically-relevant molecules known to interact with RO_2 (such as NO_3), suggest that this chemistry will remain a challenging and exciting frontier in the application of *ab initio* quantum chemistry.

Bibliography

[1] Plato, *The Republic*; Penguin Books Ltd: London, UK, 2003; p 163.

[2] Brown, T. L.; LeMay, H. E.; Bursten, B. E.; Murphy, C. J.; Woodward, P. M.; Stoltzfus, M. W. *Chemistry: The Central Science*, 14th ed.; Pearson Education: Upper Saddle River, NJ, 2017.

[3] Shavitt, I.; Bartlett, R. J. *Many-Body Methods in Chemistry and Physics: MBPT and Coupled-Cluster Theory*; Cambridge University Press: Cambridge, UK, 2009.

[4] *World Energy Outlook 2016*; International Energy Agency (IEA): Paris, France, 2016.

[5] *The World Health Report: Reducing Risks, Promoting Healthy Life*; World Health Organization (WHO): Geneva, Switzerland, 2002.

[6] Monks, P. S.; Granier, C.; Fuzzi, S.; Stohl, A.; Williams, M. L.; Akimoto, H.; Amann, M.; Baklanov, A.; Baltensperger, U.; Bey, I.; Blake, N.; Blake, R. S.; Carslaw, K.; Cooper, O. R.; Dentener, F.; Fowler, D.; Fragkou, E.; Frost, G. J.; Generoso, S.; Ginoux, P.; Grewe, V.; Guenther, A.; Hansson, H. C.; Henne, S.; Hjorth, J.; Hofzumahaus, A.; Huntrieser, H.; Isaksen, I. S. A.; Jenkin, M. E.; Kaiser, J.; Kanakidou, M.; Klimont, Z.; Kulmala, M.; Laj, P.; Lawrence, M. G.; Lee, J. D.; Liousse, C.; Maione, M.; McFiggans, G.; Metzger, A.; Mieville, A.; Moussiopoulos, N.; Orlando, J. J.; O'Dowd, C. D.; Palmer, P. I.; Parrish, D. D.; Petzold, A.; Platt, U.;

Pöschl, U.; Prévôt, A. S. H.; Reeves, C. E.; Reimann, S.; Rudich, Y.; Sellegri, K.; Steinbrecher, R.; Simpson, D.; ten Brink, H.; Theloke, J.; van der Werf, G. R.; Vautard, R.; Vestreng, V.; Vlachokostas, C.; von Glasow, R. *Atmos. Environ.* **2009**, *43*, 5268.

[7] *Burden of Disease from the Joint Effects of Household and Ambient Air Pollution for 2012*; World Health Organization (WHO): Geneva, Switzerland, 2016.

[8] Ingold, K. U. *Acc. Chem. Res.* **1969**, *2*, 1.

[9] Morley, C.; Pilling, M. J. In *Low-Temperature Combustion and Autoignition*; Pilling, M. J., Ed.; Elsevier Science: Amsterdam, The Netherlands, 1997; pp ix–xx.

[10] Nonhebel, D. C.; Tedder, J. M.; Walton, J. C. *Radicals*; Cambridge University Press: Cambridge, UK, 1979; Chapter 14, pp 150–159.

[11] Bradley, D.; Morley, C. In *Low-Temperature Combustion and Autoignition*; Pilling, M. J., Ed.; Elsevier Science: Amsterdam, The Netherlands, 1997; Chapter 7, pp 661–760.

[12] Zádor, J.; Taatjes, C. A.; Fernandes, R. X. *Prog. Energy Combust. Sci.* **2011**, *37*, 371.

[13] Lightfoot, P. D.; Cox, R. A.; Crowley, J. N.; Destriau, M.; Hayman, G. D.; Jenkin, M. E.; Moortgat, G. K.; Zabel, F. *Atmos. Environ.* **1992**, *26A*, 1805.

[14] Walker, R. W.; Morley, C. In *Low-Temperature Combustion and Autoignition*; Pilling, M. J., Ed.; Elsevier Science: Amsterdam, The Netherlands, 1997; Chapter 1, pp 1–124.

[15] Wayne, R. P. *Chemistry of Atmospheres*, 3rd ed.; Oxford University Press: Oxford, UK, 2000; Chapter 5, pp 321–480.

[16] Monks, P. S. *Chem. Soc. Rev.* **2005**, *34*, 376.

[17] Orlando, J. J.; Tyndall, G. S. *Chem. Soc. Rev.* **2012**, *41*, 6294.

[18] Tyndall, G. S.; Cox, R. A.; Granier, C.; Lesclaux, R.; Moortgat, G. K.; Pilling, M. J.; Ravishankara, A. R.; Wallington, T. J. *J. Geophys. Res.* **2001**, *106*, 12157.

[19] Vereecken, L.; Francisco, J. S. *Chem. Soc. Rev.* **2012**, *41*, 6259.

[20] Finlayson-Pitts, B. J.; Pitts, J. N. *Science* **1997**, *276*, 1045.

[21] Crutzen, P. J. *Annu. Rev. Earth Planet. Sci.* **1979**, *7*, 443.

[22] Wayne, R. P. *Chemistry of Atmospheres*, 3rd ed.; Oxford University Press: Oxford, UK, 2000; Chapter 4, pp 155–320.

[23] Atkinson, R. *Atmos. Environ.* **2000**, *34*, 2063.

[24] Seinfeld, J. H.; Pandis, S. N. *Atmospheric Chemistry and Physics: From Air Pollution to Climate Change*, 3rd ed.; John Wiley & Sons: Hoboken, NJ, 2016; p xxiii.

[25] Baulch, D. L.; Cox, R. A.; Crutzen, P. J.; Hampson, R. F.; Kerr, J. A.; Troe, J.; Watson, R. T. *J. Phys. Chem. Ref. Data* **1982**, *11*, 327.

[26] Brown, S. S.; Stutz, J. *Chem. Soc. Rev.* **2012**, *41*, 6405.

[27] Smith, I. W. M. *J. Chem. Soc., Faraday Trans.* **1991**, *87*, 2271.

[28] Baulch, D. L. In *Low-Temperature Combustion and Autoignition*; Pilling, M. J., Ed.; Elsevier Science: Amsterdam, The Netherlands, 1997; Chapter 3, pp 235–292.

[29] Pilling, M. J. *Chem. Soc. Rev.* **2008**, *37*, 676.

[30] Battin-Leclerc, F.; Blurock, E.; Bounaceur, R.; Fournet, R.; Glaude, P.-A.; Herbinet, O.; Sirjean, B.; Warth, V. *Chem. Soc. Rev.* **2011**, *40*, 4762.

[31] Copan, A. V.; Wiens, A. E.; Nowara, E. M.; Schaefer, H. F.; Agarwal, J. *J. Chem. Phys.* **2015**, *142*, 054303.

[32] Wallington, T. J.; Nielsen, O. J.; Sehested, J. In *Peroxyl Radicals*; Alfassi, Z. B., Ed.; John Wiley & Sons: Chichester, UK, 1997; Chapter 7, pp 113–172.

[33] King, M. D.; Canosa-Mas, C. E.; Wayne, R. P. *Atmos. Environ.* **2001**, *35*, 2081.

[34] King, M. D.; Thompson, K. C. *Atmos. Environ.* **2003**, *37*, 4517.

[35] Lohr, L. L.; Barker, J. R.; Shroll, R. M. *J. Phys. Chem. A* **2003**, *107*, 7429.

[36] Barker, J. R.; Lohr, L. L.; Shroll, R. M.; Reading, S. *J. Phys. Chem. A* **2003**, *107*, 7434.

[37] Zhang, J.; Dransfield, T.; Donahue, N. M. *J. Phys. Chem. A* **2004**, *108*, 9082.

[38] Zhao, Y.; Houk, K. N.; Olson, L. P. *J. Phys. Chem. A* **2004**, *108*, 5864.

[39] Cheng, X.; Zhou, Z.; Zhao, Y.; Sun, Y.; Zhu, Y. *J. Mol. Struct.* **2005**, *725*, 103.

[40] Pan, X. M.; Fu, Z.; Li, Z. S.; Sun, C. C.; Sun, H.; Su, Z. M.; Wang, R. S. *Chem. Phys. Lett.* **2005**, *409*, 98.

[41] Lesar, A.; Hodošček, M.; Drougas, E.; Kosmas, A. M. *J. Phys. Chem. A* **2006**, *110*, 7898.

[42] Arenas, J. F.; Avila, F. J.; Otero, J. C.; Peláez, D.; Soto, J. *J. Phys. Chem. A* **2008**, *112*, 249.

[43] Stimac, P. J.; Barker, J. R. *J. Phys. Chem. A* **2008**, *112*, 2553.

[44] Ravelo, R. M.; Francisco, J. S. *J. Am. Chem. Soc.* **2008**, *130*, 11234.

[45] Williams, J. E.; Le Bras, G.; Kukui, A.; Ziereis, H.; Brenninkmeijer, C. A. M. *Atmos. Chem. Phys.* **2014**, *14*, 2363.

[46] Spicer, C. W.; Villa, A.; Wiebe, H. A.; Heicklen, J. *J. Am. Chem. Soc.* **1973**, *95*, 13.

[47] Pate, C. T.; Finlayson, B. J.; Pitts, J. N. *J. Am. Chem. Soc.* **1974**, *96*, 6554.

[48] Simonaitis, R.; Heicklen, J. *J. Phys. Chem.* **1974**, *78*, 2417.

[49] Cox, R. A.; Derwent, R. G.; Holt, P. M.; Kerr, J. A. *J. Chem. Soc., Faraday Trans. 1* **1976**, *72*, 2044.

[50] Anastasi, C.; Smith, I. W. M.; Parkes, D. A. *J. Chem. Soc., Faraday Trans. 1* **1978**, *74*, 1693.

[51] Plumb, I. C.; Ryan, K. R.; Steven, J. R.; Mulcahy, M. F. R. *Chem. Phys. Lett.* **1979**, *63*, 255.

[52] Adachi, H.; Basco, N. *Chem. Phys. Lett.* **1979**, *63*, 490.

[53] Cox, R. A.; Tyndall, G. S. *Chem. Phys. Lett.* **1979**, *65*, 357.

[54] Simonaitis, R.; Heicklen, J. *Chem. Phys. Lett.* **1979**, *65*, 361.

[55] Cox, R. A.; Tyndall, G. S. *J. Chem. Soc., Faraday Trans. 2* **1980**, *76*, 153.

[56] Sander, S. P.; Watson, R. T. *J. Phys. Chem.* **1980**, *84*, 1664.

[57] Ravishankara, A. R.; Eisele, F. L.; Kreutter, N. M.; Wine, P. H. *J. Chem. Phys.* **1981**, *74*, 2267.

[58] Simonaitis, R.; Heicklen, J. *J. Phys. Chem.* **1981**, *85*, 2946.

[59] Plumb, I. C.; Ryan, K. R.; Steven, J. R.; Mulcahy, M. F. R. *J. Phys. Chem.* **1981**, *85*, 3136.

[60] Zellner, R.; Fritz, B.; Lorenz, K. *J. Atmos. Chem.* **1986**, *4*, 241.

[61] Sehested, J.; Nielsen, O. J.; Wallington, T. J. *Chem. Phys. Lett.* **1993**, *213*, 457.

[62] Masaki, A.; Tsunashima, S.; Washida, N. *Chem. Phys. Lett.* **1994**, *218*, 523.

[63] Villalta, P. W.; Huey, L. G.; Howard, C. J. *J. Phys. Chem.* **1995**, *99*, 12829.

[64] Helleis, F.; Moortgat, G. K.; Crowley, J. N. *J. Phys. Chem.* **1996**, *100*, 17846.

[65] Scholtens, K. W.; Messer, B. M.; Cappa, C. D.; Elrod, M. J. *J. Phys. Chem. A* **1999**, *103*, 4378.

[66] Goldstein, S.; Lind, J.; Merenyi, G. *J. Phys. Chem. A* **2004**, *108*, 1719.

[67] Xing, J.-H.; Nagai, Y.; Kusuhara, M.; Miyoshi, A. *J. Phys. Chem. A* **2004**, *108*, 10458.

[68] Bacak, A.; Bardwell, M. W.; Raventos, M. T.; Percival, C. J.; Sanchez-Reyna, G.; Shallcross, D. E. *J. Phys. Chem. A* **2004**, *108*, 10681.

[69] Butkovskaya, N.; Kukui, A.; Le Bras, G. *J. Phys. Chem. A* **2012**, *116*, 5972.

[70] Atkinson, R.; Carter, W. P. L.; Winer, A. M. *J. Phys. Chem.* **1983**, *87*, 2012.

[71] Atkinson, R. *Atmos. Environ.* **1990**, *24A*, 1.

[72] Atkinson, R. *J. Phys. Chem. Ref. Data* **1994**, Monograph No. 2.

[73] Carter, W. P. L.; Atkinson, R. *J. Atmos. Chem.* **1989**, *8*, 165.

[74] Orlando, J. J.; Tyndall, G. S.; Calvert, J. G. *Atmos. Environ.* **1992**, *26A*, 3111.

[75] Thompson, C. R.; Kats, G.; Lennox, R. W. *Environ. Sci. Tech.* **1979**, *13*, 1263.

[76] Chuck, A. L.; Turner, S. M.; Liss, P. S. *Science* **2002**, *297*, 1151.

[77] Ellison, G. B.; Herbert, J. M.; McCoy, A. B.; Stanton, J. F.; Szalay, P. G. *J. Phys. Chem. A* **2004**, *108*, 7639.

[78] Phillips, L.; Shaw, R. *Symp. (Int.) Combust.* **1965**, *10*, 453.

[79] Baker, G.; Shaw, R. *J. Chem. Soc.* **1965**, 6965.

[80] Wiebe, H. A.; Villa, A.; Hellman, T. M.; Heicklen, J. *J. Am. Chem. Soc.* **1973**, *95*, 7.

[81] Mendenhall, G. D.; Golden, D. M.; Benson, S. W. *Int. J. Chem. Kinet.* **1975**, *7*, 725.

[82] Barker, J. R.; Benson, S. W.; Golden, D. M. *Int. J. Chem. Kinet.* **1977**, *9*, 31.

[83] Batt, L.; Rattray, G. N. *Int. J. Chem. Kinet.* **1979**, *11*, 1183.

[84] McCaulley, J. A.; Anderson, S. M.; Jeffries, J. B.; Kaufman, F. *Chem. Phys. Lett.* **1985**, *115*, 180.

[85] Frost, M. J.; Smith, I. W. M. *J. Chem. Soc., Faraday Trans.* **1990**, *86*, 1751.

[86] Biggs, P.; Canosa-Mas, C. E.; Fracheboud, J.-M.; Parr, A. D.; Shallcross, D. E.; Wayne, R. P.; Caralp, F. *J. Chem. Soc., Faraday Trans.* **1993**, *89*, 4163.

[87] Wollenhaupt, M.; Crowley, J. N. *J. Phys. Chem. A* **2000**, *104*, 6429.

[88] Martínez, E.; Albaladejo, J.; Jiménez, E.; Notario, A.; Díaz de Mera, Y. *Chem. Phys. Lett.* **2000**, *329*, 191.

[89] Kukui, A.; Bossoutrot, V.; Laverdet, G.; Le Bras, G. *J. Phys. Chem. A* **2000**, *104*, 935.

[90] Carbajo, P. G.; Orr-Ewing, A. J. *Phys. Chem. Chem. Phys.* **2010**, *12*, 6084.

[91] Chai, J.; Hu, H.; Dibble, T. S.; Tyndall, G. S.; Orlando, J. J. *J. Phys. Chem. A* **2014**, *118*, 3552.

[92] Chai, J.; Dibble, T. S. *Int. J. Chem. Kinet.* **2014**, *46*, 501.

[93] Raghavachari, K.; Trucks, G. W.; Pople, J. A.; Head-Gordon, M. *Chem. Phys. Lett.* **1989**, *157*, 479.

[94] Hampel, C.; Peterson, K. A.; Werner, H.-J. *Chem. Phys. Lett.* **1992**, *190*, 1.

[95] Watts, J. D.; Gauss, J.; Bartlett, R. J. *Chem. Phys. Lett.* **1992**, *200*, 1.

[96] Watts, J. D.; Gauss, J.; Bartlett, R. J. *J. Chem. Phys.* **1993**, *98*, 8718.

[97] Deegan, M. J. O.; Knowles, P. J. *Chem. Phys. Lett.* **1994**, *227*, 321.

[98] Stanton, J. F. *Chem. Phys. Lett.* **1997**, *281*, 130.

[99] Dunning, T. H. *J. Chem. Phys.* **1989**, *90*, 1007.

[100] Allinger, N. L.; Fermann, J. T.; Allen, W. D.; Schaefer, H. F. *J. Chem. Phys.* **1997**, *106*, 5143.

[101] Császár, A. G.; Allen, W. D.; Schaefer, H. F. *J. Chem. Phys.* **1998**, *108*, 9751.

[102] Császár, A. G.; Tarczay, G.; Leininger, M. L.; Polyansky, O. L.; Tennyson, J.; Allen, W. D. In *Spectroscopy from Space*; Demaison, J., Sarka, K., Eds.; Kluwer Academic Publishers: Dordrecht, The Netherlands, 2001; Chapter 19, pp 317–340.

[103] Gonzales, J. M.; Pak, C.; Cox, R. S.; Allen, W. D.; Schaefer, H. F.; Császár, A. G.; Tarczay, G. *Chem. Eur. J.* **2003**, *9*, 2173.

[104] Feller, D. *J. Chem. Phys.* **1993**, *98*, 7059.

[105] Helgaker, T.; Klopper, W.; Koch, H.; Noga, J. *J. Chem. Phys.* **1997**, *106*, 9639.

[106] Bomble, Y. J.; Stanton, J. F.; Kállay, M.; Gauss, J. *J. Chem. Phys.* **2005**, *123*, 054101.

[107] Kállay, M.; Gauss, J. *J. Chem. Phys.* **2005**, *123*, 214105.

[108] Kállay, M.; Gauss, J. *J. Chem. Phys.* **2008**, *129*, 144101.

[109] Woon, D. E.; Dunning, T. H. *J. Chem. Phys.* **1995**, *103*, 4572.

[110] Sellers, H.; Pulay, P. *Chem. Phys. Lett.* **1984**, *103*, 463.

[111] Handy, N. C.; Yamaguchi, Y.; Schaefer, H. F. *J. Chem. Phys.* **1986**, *84*, 4481.

[112] Cowan, R. D.; Griffin, D. C. *J. Opt. Soc. Am.* **1976**, *66*, 1010.

[113] Perera, S. A.; Bartlett, R. J. *Chem. Phys. Lett.* **1993**, *216*, 606.

[114] Klopper, W. *J. Comput. Chem.* **1997**, *18*, 20.

[115] Saeh, J. C.; Stanton, J. F. *J. Chem. Phys.* **1999**, *111*, 8275.

[116] Stanton, J. F. *J. Chem. Phys.* **2001**, *115*, 10382.

[117] Szalay, P. G.; Vázquez, J.; Simmons, C.; Stanton, J. F. *J. Chem. Phys.* **2004**, *121*, 7624.

[118] Crawford, T. D.; Stanton, J. F.; Allen, W. D.; Schaefer, H. F. *J. Chem. Phys.* **1997**, *107*, 10626.

[119] Lee, T. J.; Taylor, P. R. *Int. J. Quantum Chem. Symp.* **1989**, *36*, 199.

[120] Jayatilaka, D.; Lee, T. J. *J. Chem. Phys.* **1993**, *98*, 9734.

[121] MOLPRO, version 2010.1, a package of *ab initio* programs written by H.-J. Werner, P. J. Knowles, G. Knizia, F. R. Manby, M. Schütz, P. Celani, T. Korona, R. Lindh, A. Mitrushenkov, G. Rauhut, K. R. Shamasundar, T. B. Adler, R. D. Amos, A. Bernhardsson, A. Berning, D. L. Cooper, M. J. O. Deegan, A. J. Dobbyn, F. Eckert,

E. Goll, C. Hampel, A. Hesselmann, G. Hetzer, T. Hrenar, G. Jansen, C. Köppl, Y. Liu, A. W. Lloyd, R. A. Mata, A. J. May, S. J. McNicholas, W. Meyer, M. E. Mura, A. Nicklaß, D. P. O'Neill, P. Palmieri, D. Peng, K. Pflüger, R. Pitzer, M. Reiher, T. Shiozaki, H. Stoll, A. J. Stone, R. Tarroni, T. Thorsteinsson, M. Wang, and A. Wolf, see http://www.molpro.net.

[122] Schmidt, M. W.; Baldridge, K. K.; Boatz, J. A.; Elbert, S. T.; Gordon, M. S.; Jensen, J. H.; Koseki, S.; Matsunaga, N.; Nguyen, K. A.; Su, S.; Windus, T. L.; Dupuis, M.; Montgomery, J. A. *J. Comput. Chem.* **1993**, *14*, 1347.

[123] Gordon, M. S.; Schmidt, M. W. In *Theory and Applications of Computational Chemistry: the First Forty Years*; Dykstra, C. E., Frenking, G., Kim, K. S., Scuseria, G. E., Eds.; Elsevier: Amsterdam, The Netherlands, 2005; pp 1167–1189.

[124] CFOUR, a quantum chemical program package written by J. F. Stanton, J. Gauss, M. E. Harding, P. G. Szalay with contributions from A. A. Auer, R. J. Bartlett, U. Benedikt, C. Berger, D. E. Bernholdt, Y. J. Bomble, L. Cheng, O. Christiansen, M. Heckert, O. Heun, C. Huber, T.-C. Jagau, D. Jonsson, J. Jusélius, K. Klein, W. J. Lauderdale, D. A. Matthews, T. Metzroth, L. A. Mück, D. P. O'Neill, D. R. Price, E. Prochnow, C. Puzzarini, K. Ruud, F. Schiffmann, W. Schwalbach, C. Simmons, S. Stopkowicz, A. Tajti, J. Vázquez, F. Wang, J. D. Watts and the integral packages MOLECULE (J. Almlöf and P. R. Taylor), PROPS (P. R. Taylor), ABACUS (T. Helgaker, H. J. Aa. Jensen, P. Jørgensen, and J. Olsen), and ECP routines by A. V. Mitin and C. van Wüllen. For the current version, see http://www.cfour.de.

[125] MRCC, a quantum chemical program suite written by M. Kállay, Z. Rolik, J. Csontos, I. Ladjánszki, L. Szegedy, B. Ladóczki, G. Samu, K. Petrov, M. Farkas, P. Nagy, D. Mester, and B. Hégely. See also Refs. 126 and 127, as well as http://www.mrcc.hu.

[126] Kállay, M.; Surján, P. R. *J. Chem. Phys.* **2001**, *115*, 2945.

[127] Rolik, Z.; Szegedy, L.; Ladjánszki, I.; Ladóczki, B.; Kállay, M. *J. Chem. Phys.* **2013**, *139*, 094105.

[128] Tsai, J.-H. M.; Harrison, J. G.; Martin, J. C.; Hamilton, T. P.; van der Woerd, M.; Jablonsky, M. J.; Beckman, J. S. *J. Am. Chem. Soc.* **1994**, *116*, 4115.

[129] Correra, T. C.; Riveros, J. M. *J. Phys. Chem. A* **2010**, *114*, 11910.

[130] de Souza, M. A. F.; Correra, T. C.; Riveros, J. M.; Longo, R. L. *J. Am. Chem. Soc.* **2012**, *134*, 19004.

[131] Proenza, Y. G.; de Souza, M. A. F.; Ventura, E.; do Monte, S. A.; Longo, R. L. *Phys. Chem. Chem. Phys.* **2014**, *16*, 26769.

[132] Watts, J. D.; Urban, M.; Bartlett, R. J. *Theor. Chim. Acta* **1995**, *90*, 341.

[133] Irikura, K. K. *J. Phys. Chem. Ref. Data* **2007**, *36*, 389.

[134] Lafferty, W. J.; Sams, R. L. *J. Mol. Spec.* **1977**, *66*, 478.

[135] Launder, A. M.; Agarwal, J.; Schaefer, H. F. *J. Chem. Phys.* **2015**, *143*, 234302.

[136] Wallington, T. J.; Dagaut, P.; Kurylo, M. J. *Chem. Rev.* **1992**, *92*, 667.

[137] Jafri, J. A.; Phillips, D. H. *J. Am. Chem. Soc.* **1990**, *112*, 2586.

[138] Nielsen, O. J.; Wallington, T. J. In *Peroxyl Radicals*; Alfassi, Z. B., Ed.; John Wiley & Sons: Chichester, UK, 1997; Chapter 5, pp 69–80.

[139] Sharp, E. N.; Rupper, P.; Miller, T. A. *Phys. Chem. Chem. Phys.* **2008**, *10*, 3955.

[140] Marić, D.; Crowley, J. N.; Burrows, J. P. *J. Phys. Chem. A* **1997**, *101*, 2561.

[141] Ase, P.; Bock, W.; Snelson, A. *J. Phys. Chem.* **1986**, *90*, 2099.

[142] Cyvin, B. N.; Cyvin, S. J.; Snelson, A. *Z. Anorg. Allg. Chem.* **1986**, *542*, 193.

[143] Chettur, G.; Snelson, A. *J. Phys. Chem.* **1987**, *91*, 913.

[144] Chettur, G.; Snelson, A. *J. Phys. Chem.* **1987**, *91*, 3483.

[145] Chettur, G.; Snelson, A. *J. Phys. Chem.* **1987**, *91*, 5873.

[146] Hunziker, H. E.; Wendt, H. R. *J. Chem. Phys.* **1976**, *64*, 3488.

[147] O'Keefe, A.; Deacon, D. A. G. *Rev. Sci. Instrum.* **1988**, *59*, 2544.

[148] Scherer, J. J.; Paul, J. B.; O'Keefe, A.; Saykally, R. J. *Chem. Rev.* **1997**, *97*, 25.

[149] Morrison, A. M.; Agarwal, J.; Schaefer, H. F.; Douberly, G. E. *J. Phys. Chem. A* **2012**, *116*, 5299.

[150] Agarwal, J.; Simmonett, A. C.; Schaefer, H. F. *Mol. Phys.* **2012**, *110*, 2419.

[151] Copan, A. V.; Schaefer, H. F.; Agarwal, J. *Mol. Phys.* **2015**, *113*, 2992.

[152] Elliott, S. N.; Turney, J. M.; Schaefer, H. F. *RSC Adv.* **2015**, *5*, 107254.

[153] Hoobler, P. R.; Turney, J. M.; Schaefer, H. F. *J. Chem. Phys.* **2016**, *145*, 174301.

[154] Blanksby, S. J.; Ramond, T. M.; Davico, G. E.; Nimlos, M. R.; Kato, S.; Bierbaum, V. M.; Lineberger, W. C.; Ellison, G. B.; Okumura, M. *J. Am. Chem. Soc.* **2001**, *123*, 9585.

[155] Mah, D. A.; Cabrera, J.; Nation, H.; Ramos, M.; Sharma, S.; Nickolaisen, S. L. *J. Phys. Chem. A* **2003**, *107*, 4354.

[156] Pushkarsky, M. B.; Zalyubovsky, S. J.; Miller, T. A. *J. Chem. Phys.* **2000**, *112*, 10695.

[157] Atkinson, D. B.; Spillman, J. L. *J. Phys. Chem. A* **2002**, *106*, 8891.

[158] Rupper, P.; Sharp, E. N.; Tarczay, G.; Miller, T. A. *J. Phys. Chem. A* **2007**, *111*, 832.

[159] Just, G. M. P.; Rupper, P.; Miller, T. A.; Meerts, W. L. *J. Chem. Phys.* **2009**, *131*, 184303.

[160] Melnik, D.; Chhantyal-Pun, R.; Miller, T. A. *J. Phys. Chem. A* **2010**, *114*, 11583.

[161] Melnik, D.; Thomas, P. S.; Miller, T. A. *J. Phys. Chem. A* **2011**, *115*, 13931.

[162] Melnik, D.; Miller, T. A. *J. Chem. Phys.* **2013**, *139*, 094201.

[163] Wagner, A. F.; Slagle, I. R.; Sarzynski, D.; Gutman, D. *J. Phys. Chem.* **1990**, *94*, 1853.

[164] Quelch, G. E.; Gallo, M. M.; Schaefer, H. F. *J. Am. Chem. Soc.* **1992**, *114*, 8239.

[165] Quelch, G. E.; Gallo, M. M.; Shen, M.; Xie, Y.; Schaefer, H. F.; Moncrieff, D. *J. Am. Chem. Soc.* **1994**, *116*, 4953.

[166] Ignatyev, I. S.; Xie, Y.; Allen, W. D.; Schaefer, H. F. *J. Chem. Phys.* **1997**, *107*, 141.

[167] Stark, M. S. *J. Am. Chem. Soc.* **2000**, *122*, 4162.

[168] Miller, J. A.; Klippenstein, S. J.; Robertson, S. H. *Proc. Combust. Inst.* **2000**, *28*, 1479.

[169] Rienstra-Kiracofe, J. C.; Allen, W. D.; Schaefer, H. F. *J. Phys. Chem. A* **2000**, *104*, 9823.

[170] Miller, J. A.; Klippenstein, S. J. *Int. J. Chem. Kinet.* **2001**, *33*, 654.

[171] Carstensen, H.-H.; Naik, C. V.; Dean, A. M. *J. Phys. Chem. A* **2005**, *109*, 2264.

[172] Wilke, J. J.; Allen, W. D.; Schaefer, H. F. *J. Chem. Phys.* **2008**, *128*, 074308.

[173] Boyd, S. L.; Boyd, R. J.; Barclay, L. R. C. *J. Am. Chem. Soc.* **1990**, *112*, 5724.

[174] Aplincourt, P.; Ruiz-López, M. F.; Assfeld, X.; Bohr, F. *J. Comput. Chem.* **1999**, *20*, 1039.

[175] Brinck, T.; Lee, H.-N.; Jonsson, M. *J. Phys. Chem. A* **1999**, *103*, 7094.

[176] Xu, W.; Lu, G. *J. Phys. Chem. A* **2008**, *112*, 6999.

[177] Sharma, S.; Raman, S.; Green, W. H. *J. Phys. Chem. A* **2010**, *114*, 5689.

[178] Miyoshi, A. *J. Phys. Chem. A* **2011**, *115*, 3301.

[179] Villano, S. M.; Huynh, L. K.; Carstensen, H.-H.; Dean, A. M. *J. Phys. Chem. A* **2011**, *115*, 13425.

[180] Almlöf, J.; Taylor, P. R. *J. Chem. Phys.* **1987**, *86*, 4070.

[181] McCaslin, L.; Stanton, J. *Mol. Phys.* **2013**, *111*, 1492.

[182] Turney, J. M.; Simmonett, A. C.; Parrish, R. M.; Hohenstein, E. G.; Evangelista, F. A.; Fermann, J. T.; Mintz, B. J.; Burns, L. A.; Wilke, J. J.; Abrams, M. L.; Russ, N. J.; Leininger, M. L.; Janssen, C. L.; Seidl, E. T.; Allen, W. D.; Schaefer, H. F.; King, R. A.; Valeev, E. F.; Sherrill, C. D.; Crawford, T. D. *WIREs Comput. Mol. Sci.* **2012**, *2*, 556.

[183] Nielsen, H. H. *Rev. Mod. Phys.* **1951**, *23*, 90.

[184] Mills, I. M. In *Molecular Spectroscopy: Modern Research*; Rao, K. N., Mathews, C. W., Eds.; Academic Press: New York, NY, 1972; Chapter 3.2, pp 115–140.

[185] Clabo, D. A.; Allen, W. D.; Remington, R. B.; Yamaguchi, Y.; Schaefer, H. F. *Chem. Phys.* **1988**, *123*, 187.

[186] Gauss, J.; Stanton, J. F. *Chem. Phys. Lett.* **1997**, *276*, 70.

[187] Nielsen, H. H. *Phys. Rev.* **1945**, *68*, 181.

[188] PyVPT2 is a vibrational anharmonicity program written in Python by J. Agarwal. Center for Computational Quantum Chemistry, University of Georgia, Athens, GA.

[189] Martin, J. M. L. *Mol. Phys.* **2014**, *112*, 785.

[190] Dyall, K. G. *J. Chem. Phys.* **2001**, *115*, 9136.

[191] Kutzelnigg, W.; Liu, W. *J. Chem. Phys.* **2005**, *123*, 241102.

[192] Liu, W.; Peng, D. *J. Chem. Phys.* **2009**, *131*, 031104.

[193] Foldy, L. L.; Wouthuysen, S. A. *Phys. Rev.* **1950**, *78*, 29.

[194] Verma, P.; Derricotte, W. D.; Evangelista, F. A. *J. Chem. Theory Comput.* **2016**, *12*, 144.

[195] Tuckett, R. P.; Freedman, P. A.; Jones, W. J. *Mol. Phys.* **1979**, *37*, 403.

[196] Jacox, M. E. *J. Phys. Chem. Ref. Data* **2003**, *32*, 1.

[197] Fink, E. H.; Ramsay, D. A. *J. Mol. Spec.* **1997**, *185*, 304.